Trade names and trademarks are used in this report for identification only. Their usage does not constitute an official endorsement, either expressed or implied, by the National Aeronautics and Space Administration.

Science
AAAS

Noble gases and nitrogen in Ryugu grains – Records of its past and recent geological activity

Short title: Noble gases and nitrogen in Ryugu grains

Authors: Ryuji Okazaki[1*], Bernard Marty[2], Henner Busemann[3], Ko Hashizume[4], Jamie D. Gilmour[5], Alex Meshik[6], Toru Yada[7], Fumio Kitajima[1], Michael W. Broadley[2], David Byrne[2], Evelyn Füri[2], My E.I. Riebe[3], Daniela Krietsch[3], Colin Maden[3], Akizumi Ishida[8], Patricia Clay[5], Sarah A. Crowther[5], Lydia Fawcett[5], Thomas Lawton[5], Olga Pravdivtseva[6], Yayoi N. Miura[9], Jisun Park[10,11], Ken-ichi Bajo[12], Yoshinori Takano[13], Keita Yamada[14], Shinsuke Kawagucci[15,16], Yohei Matsui[15,16], Mizuki Yamamoto[1], Kevin Righter[17], Saburo Sakai[13], Naoyoshi Iwata[18], Naoki Shirai[19,20], Shun Sekimoto[21], Makoto Inagaki[21], Mitsuru Ebihara[22], Reika Yokochi[23], Kunihiko Nishiizumi[24], Keisuke Nagao[25], Jong Ik Lee[25], Akihiro Kano[26], Marc W. Caffee[27,28], Ryu Uemura[29], Tomoki Nakamura[8], Hiroshi Naraoka[1], Takaaki Noguchi[30,31], Hikaru Yabuta[32], Hisayoshi Yurimoto[12], Shogo Tachibana[33], Hirotaka Sawada[7], Kanako Sakamoto[7], Masanao Abe[7], Masahiko Arakawa[34], Atsushi Fujii[7], Masahiko Hayakawa[7], Naoyuki Hirata[34], Naru Hirata[35], Rie Honda[36], Chikatoshi Honda[35], Satoshi Hosoda[7], Yu-ichi Iijima[7†], Hitoshi Ikeda[7], Masateru Ishiguro[37], Yoshiaki Ishihara[38], Takahiro Iwata[7], Kosuke Kawahara[7], Shota Kikuchi[39], Kohei Kitazato[35], Koji Matsumoto[40,41], Moe Matsuoka[42], Tatsuhiro Michikami[43], Yuya Mimasu[7], Akira Miura[7], Tomokatsu Morota[26], Satoru Nakazawa[7], Noriyuki Namiki[40,41], Hirotomo Noda[40,41], Rina Noguchi[44], Naoko Ogawa[7], Kazunori Ogawa[7], Tatsuaki Okada[7], Chisato Okamoto[34†], Go Ono[7], Masanobu Ozaki[7,41], Takanao Saiki[7], Naoya Sakatani[45], Hiroki Senshu[39], Yuri Shimaki[7], Kei Shirai[7,34], Seiji Sugita[26], Yuto Takei[7], Hiroshi Takeuchi[7], Satoshi Tanaka[7], Eri Tatsumi[26,46], Fuyuto Terui[47], Ryudo Tsukizaki[7], Koji Wada[39], Manabu Yamada[39], Tetsuya Yamada[7], Yukio Yamamoto[7], Hajime Yano[7], Yasuhiro Yokota[7], Keisuke Yoshihara[7], Makoto Yoshikawa[7], Kent Yoshikawa[7], Shizuho Furuya[7], Kentaro Hatakeda[48], Tasuku Hayashi[7], Yuya Hitomi[48], Kazuya Kumagai[48], Akiko Miyazaki[7], Aiko Nakato[7], Masahiro Nishimura[7], Hiromichi Soejima[48], Ayako Iwamae[48], Daiki Yamamoto[7,49], Kasumi Yogata[7], Miwa Yoshitake[7], Ryota Fukai[7], Tomohiro Usui[7], Harold C. Connolly Jr.[50], Dante Lauretta[51], Sei-ichiro Watanabe[29], and Yuichi Tsuda[7].

Affiliations:

[1]Department of Earth and Planetary Sciences, Kyushu University, Fukuoka, 819-0395, Japan.

[2]Université de Lorraine, CNRS, CRPG, F-54000 Nancy, France.

[3]Institute of Geochemistry and Petrology, ETH Zürich, 8092 Zürich, Switzerland.

[4]Faculty of Science, Ibaraki University, Mito, 310-8512, Japan.

[5]Department of Earth and Environmental Sciences, The University of Manchester, Manchester M13 9PL, UK.

[6]Physics Department, Washington University, Saint Louis, MO, 63130, USA.

[7]Institute of Space and Astronautical Science (ISAS), Japan Aerospace Exploration Agency (JAXA), Sagamihara, 252-5210, Japan.

[8]Department of Earth Science, Tohoku University, Sendai, 980-8578, Japan.

[9]Earthquake Research Institute, University of Tokyo, Tokyo, 113-0032, Japan.

[10]Physical Sciences, Kingsborough Community College, Brooklyn, NY, 11235, USA.

[11]Department of Earth and Planetary Sciences, American Museum of Natural History, NY, 10024, USA.

[12]Department of Earth and Planetary Sciences, Hokkaido University, Sapporo, 060-0810, Japan.

[13]Biogeochemistry Research Center (BGC), Japan Agency for Marine-Earth Science and Technology (JAMSTEC), Yokosuka, 237-0061, Japan.

[14]Department of Chemical Science and Engineering, Tokyo Institute of Technology, Yokohama, 226-8503, Japan.

[15]Research Institute for Global Change, JAMSTEC, Yokosuka, 237-0061, Japan.

[16]Institute for Extra-cutting-edge Science and Technology Avant-garde Research (X-star), JAMSTEC, Yokosuka, 237-0061, Japan.

[17]ARES, Mailcode XI2, NASA Johnson Space Center, 2101 NASA Parkway, Houston, TX, 77058, USA.

[18]Faculty of Science, Yamagata University, Yamagata, 990-8560, Japan.

[19]Graduate School of Science and Engineering, Tokyo Metropolitan University, Hachioji, 192-0397, Japan.

[20]Department of Chemistry, Faculty of Science, Kanagawa University, Hiratsuka, Kanagawa, 259-1293, Japan.

[21]Institute for Integrated Radiation and Nuclear Science, Kyoto University, Osaka, 590-0494, Japan.

[22]Department of Earth Sciences, Waseda University, Tokyo, 169- 8050, Japan.

[23]Origins Laboratory, Department of the Geophysical Sciences and Enrico Fermi Institute, The University of Chicago, Chicago IL, USA.

[24]Space Sciences Laboratory, University of California, Berkeley, CA, 94720, USA.

[25]Division of Earth Sciences, Korea Polar Research Institute, Incheon, 21990, Korea.

[26]Department of Earth and Planetary Science, University of Tokyo, Tokyo, 113-0033, Japan.

[27]Department of Physics and Astronomy, Purdue University, West Lafayette, IN 47907, USA.

[28]Department of Earth, Atmospheric, and Planetary Sciences, Purdue University, West Lafayette, IN 47907, USA.

[29]Department of Earth and Environmental Sciences, Nagoya University; Nagoya, 464-8601, Japan.

[30]Division of Earth and Planetary Sciences, Kyoto University, Kyoto, 606-8502, Japan.

[31]Faculty of Arts and Science, Kyushu University, Fukuoka, 819-0395, Japan.

[32]Department of Earth and Planetary Systems Science, Hiroshima University, Higashi-Hiroshima, 739-8526, Japan.

[33]UTokyo Organization for Planetary and Space Science, The University of Tokyo, Tokyo, 113-0033, Japan.

[34]Center for Planetary Science, Kobe University, Kobe, 657-8501, Japan.

[35]Aizu Research Cluster for Space Science, University of Aizu, Aizu-Wakamatsu, 965-8580, Japan.

[36]Department of Information Science, Kochi University, Kochi, 780-8520, Japan.

[37]Department of Physics and Astronomy, Seoul National University, Seoul, 08826, Republic of Korea.

[38]JAXA Space Exploration Center (JSEC), JAXA, Sagamihara, 252-5210, Japan.

[39]Planetary Exploration Research Center, Chiba Institute of Technology, Narashino, 275-0016, Japan.

[40]RISE Project, National Astronomical Observatory of Japan, Mitaka, 181-8588, Japan.

[41]The Graduate University for Advanced Studies, SOKENDAI, Shonan Village, Hayama, Kanagawa, 240-0193, Japan.

[42]Geological Survey of Japan (GSJ), National Institute of Advanced Industrial Science and Technology (AIST), Ibaraki, 305-8567, Japan.

[43]Faculty of Engineering, Kindai University, Higashi-Hiroshima, 739-2116, Japan.

[44]Faculty of Science, Niigata University, Niigata, 950-2181, Japan.

[45]Department of Physics, Rikkyo University, Tokyo, 171-8501, Japan.

[46]Instituto de Astrofísica de Canarias, University of La Laguna, Tenerife, Spain.

[47]Department of Mechanical Engineering, Kanagawa Institute of Technology, Atsugi, 243-0292, Japan.

[48]Marine Works Japan Ltd., Yokosuka, 237-0063, Japan.

[49]Department of Earth and Planetary Science, Tokyo Institute of Technology, Ookayama, Tokyo, 152-8550, Japan.

[50]Department of Geology, School of Earth and Environment, Rowan University, Glassboro, NJ, 08028, USA.

[51]Lunar and Planetary Laboratory, University of Arizona, Tucson, AZ, 85705, USA.

***Corresponding author. E-mail: okazaki.ryuji.703@m.kyushu-u.ac.jp**

†Deceased.

Abstract:

Noble gas and nitrogen isotopes in individual grains sampled by the Hayabusa2 spacecraft from asteroid (162173) Ryugu are dominated by presolar and primordial components that were trapped into various Ryugu's ingredients before or after the solar system formation. The concentrations of the primordial noble gases are comparable to or higher than those in CI chondrites, the chemically most primitive meteorites. Various nitrogen carriers with different isotopic ratios exist, as indicated by heterogeneous concentrations and isotopic ratios among the samples. Cosmic-ray exposure ages of ~5 Myr and the rare signs of the solar wind record the recent regolith evolution after the transit to near-Earth orbit. The volatile compositions of the Ryugu grains record the origin of the source materials and the recent geological activity of Ryugu.

One-Sentence Summary:

We present the first results of noble gas and nitrogen isotope analyses of Ryugu grains returned by the Hayabusa2 spacecraft.

Main Text:

The Hayabusa2 spacecraft returned to Earth on December 6, 2020, after successfully collecting surface and subsurface materials from asteroid (162173) Ryugu (*1*), a C-type asteroid thought to have chemical and mineralogical compositions similar to carbonaceous chondrites (*2*). Carbonaceous chondrites contain abundant volatile elements and molecules, such as hydrogen, carbon, nitrogen, noble gases, and organic compounds. As such they may be an important source of volatiles delivered to Earth and the other terrestrial planets (*3, 4*). Nitrogen and noble gases in different carbonaceous chondrites show significant variations in their chemical and isotopic abundances. The diversity is thought to be primarily inherited from primordial source materials but may also record many of processes occurring in the interior of parent bodies after the accretion, such as thermal metamorphism and aqueous alteration (*5, 6*).

In addition to providing insight into the chemical make-up of the parent body and the subsequent processes that may have occurred during thermal and aqueous alterations, noble gas isotopes can be used to assess asteroid surface activities, e.g., degrees and durations of meteorite bombardments, gardening, brecciation, and solar/galactic energetic-particle irradiation. Remote-sensing observations by Hayabusa2 revealed signs of meteoritic bombardment, space weathering, and heating in Ryugu (*7–10*). Based on noble gas isotopes originating from solar wind (SW) implantation, and those produced by galactic cosmic rays (GCRs) and solar cosmic rays (SCRs) via spallation/neutron capture reactions, we can trace the duration and conditions of SW and cosmic ray exposures. These exposure durations may play an important role in possible alterations of surficial materials, because energetic particle irradiation could cause alteration of susceptible materials, such as organics, which affects the interpretation of their evolution history.

Here, we present the first report of abundances and isotopic compositions of nitrogen and noble gases in solid grains returned by JAXA from asteroid Ryugu. Ryugu's source materials, parent body processes, orbital evolution, and Ryugu surface activities will be discussed.

Individual-grain analyses by a combination of non-destructive observations and destructive isotope measurements

We measured noble gas and nitrogen isotopes in 21 individual Ryugu grains (Table S1), typically 0.8 mm-sized, not clumps of powders, that were collected during the 1st and 2nd touchdown (TD) operations. The samples of the 1st TD (hereafter denoted Ryugu-A samples, A0105-series) were collected from surface layer of Ryugu and stored in Chamber A of the sample catcher, while the 2nd TD samples were collected from subsurface layer and stored in Chamber C (denoted Ryugu-C samples, C0106-series) (*11, 12*). Because asteroid surface materials are generally breccia consisting of different lithologies, we carried out a combination analysis of non-destructive analyses, as well as conventional isotope analyses that are destructive, but have advantages in their high-precision determination of absolute abundances and isotope ratios of volatile components. For the non-destructive observations before destructive isotope analyses, each of the samples was pressed onto diamond disks and pelletized to obtain a flat surface (*13*). Fourier-Transform Infrared (FT-IR) spectroscopy and Field-Emission Scanning Electron Microscope (FESEM) observations were performed with greatest attention to contamination and sample damage due to photon and electron exposures (*13*). After these examinations, abundances and isotopic compositions of noble gases and nitrogen were measured in individual Ryugu pelletized samples in several laboratories (Fig. S1). The total (i.e., organic and inorganic) carbon content was also determined for two samples (A0105-07 and C0106-07) based on the CO_2 pressure evolved during the combustion (*13*). It should be emphasized that the pelletized samples were treated without exposure to Earth's

atmosphere throughout the entire processes, including sample preparation, transportation, weighing, and introduction to the instruments for all analyses (*13*). The fragments of material generated during pelletization were also collected and prepared for noble gas analyses, albeit in atmosphere (*13* and Table S1).

Mineralogical/petrographic and spectroscopic similarities with CI chondrites

The FESEM observation shows that the pelletized Ryugu grains are mainly composed of fine-grained matrices, in which phyllosilicates occur as the major mineral phase (Figs. 1, S2, and S3). The modal abundances of magnetite and sulfide grains in Ryugu-A samples are similar to those of Ryugu-C samples, and both are similar to those in CI chondrites (*13*), but are distinct from those in CM and dehydrated CI-like carbonaceous chondrites (*14*).

The FT-IR spectra of our Ryugu samples show O-H stretching of phyllosilicates (*15*) at 3698.8 cm^{-1} (2.70 μm) and C-H stretching (*15*) at 2968.4 cm^{-1} (3.37 μm) (Fig. 2), which is consistent with the results reported for the bulk Ryugu samples (e.g., *12*). These results indicate a close relationship between Ryugu and CI chondrites, which is consistent with the observations from other techniques (*16–19*). Further spectral features are presented in Figs. S4 and S5.

These FESEM and FT-IR studies indicate that our samples are typical Ryugu samples with a CI lithology, containing no clasts with CM or dehydrated CI-like chondrite characteristics (*14*).

Noble gas isotopic compositions

The bulk isotopic ratios of He can be explained by superpositions of primordially trapped He, i.e., the so-called P1, (or "Q" gas, residing in an enigmatic [most likely carbonaceous] carrier phase, Q: *20, 21*) and presolar HL (carried by presolar nano-diamonds: *21*), along with SW (*22*), and SCR/GCR-produced (cosmogenic) components (Fig. S6). Most of the samples appear to contain HL-Ne and P1-Ne as the major Ne components (Fig. 3A), though it is difficult to determine their relative abundances, which affect the estimation of SW-Ne abundances. Although the presence of implantation-fractionated SW (FSW: *23*) cannot be ruled out, elemental abundances of the Ryugu samples (Fig. S7A) are consistent with the mixing between the HL and P1. Two samples (A0105-01 and C0106-06) record contributions from presolar G- and/or R-Ne components (essentially pure ^{22}Ne carried by presolar graphite/SiC and graphite, respectively: *21*) as revealed by the stepped heating Ne data (Fig. 3B and Table S2). Only A0105-06 and A0105-15 show a clear contribution of SW-Ne in their bulk compositions (Fig. 3A), in contrast to the rest of samples, which only show a minor contribution from SW, if at all, in their step heating data (Fig. 3B).

The $^{38}Ar/^{36}Ar$ ratios of the bulk Ryugu samples range between 0.186±0.001 and 0.194±0.007 (Table S2), which are similar to the corresponding value of P1 (0.188: *20*) or other trapped components. The SW-rich samples also show this range of $^{38}Ar/^{36}Ar$ (Table S2). The higher $^{38}Ar/^{36}Ar$ ratios (>0.188) are not correlated to cosmogenic ^{21}Ne abundances, which may be due to higher abundances of the target elements for cosmogenic ^{38}Ar, such as K and Ca, in some of the samples. The bulk $^{40}Ar/^{36}Ar$ ratios range from 4 to 70, probably with large contributions of the instrumental blank due to the small amounts of ^{40}Ar in the Ryugu samples. Bulk ^{40}Ar concentrations were variable from 1 to 5×10^{-5} cm^3 STP (Standard Temperature and Pressure) /g after blank correction, suggesting heterogeneously distributed potassium in the samples and variable atmospheric contamination from the instrument.

Isotopic ratios of Xe are interpreted to be dominated by P1 with variable contributions of HL and SW components (Fig. S8 and Table S2), although a small contribution from terrestrial atmosphere cannot be excluded. Some of the samples may have cosmogenic contributions, but

large uncertainties and the dominant presence of trapped Xe preclude unambiguous identification of their presence. Sample A0105-15 (rich in SW-Ne) has a Xe composition similar to that of SW-Xe in ^{130}Xe to ^{136}Xe isotopes, (Fig. S8) but is depleted in ^{124}Xe and ^{126}Xe isotopes (Table S2). Excesses in ^{129}Xe from the decay of short-lived ^{129}I with ^{129}Xe/^{132}Xe >1.042 of (^{129}Xe/^{132}Xe)$_{P1}$ (*20*) are observed in some samples. Isotopic ratios of Kr are dominated by the P1 and SW components (Fig. S9). Some variations from P1 are observed for Kr and Xe isotopes, likely due to interferences from hydrocarbons which can significantly affect the less abundant Kr and Xe isotopes when measuring such small sample masses (Figs. S8 and S9).

Nitrogen abundances and isotopic composition

The bulk δ^{15}N values of A0105-07 and C0106-07 are +1.02 and -0.16 ‰, respectively, and are low compared to the other Ryugu samples (+39–+43 ‰, observed range in C-rich grains: *18*; +43.0 ± 9.0 ‰, averaged value for mg-sized aggregates: *19*) and CI chondrite values (+31–+52 ‰: *24–28*), but similar to that of the dehydrated CI chondrite Yamato (Y)-980115 (-2.8 ‰: *29*) (Fig. 4). The bulk δ^{15}N of A0105-05 and C0106-06 are between the other two samples (A0105-07 and C0106-07) and CI chondrites (Fig. 4). The nitrogen contents in our samples are between 700 and 900 ppm (Table S3), 2–3 times lower than the CI values (*24–28*), but similar to that of the dehydrated CI chondrite Y-980115 (*29*) and the highly altered CM1 chondrite Meteorite Hills MET 01070 (*28*) (Fig. 4). A linear trend is observed in the nitrogen isotope ratios and inverse of the nitrogen concentrations (Fig. 4), suggesting the presence of at least two indigenous end members; one with a δ^{15}N value as high as +70 ‰, and the other with a δ^{15}N value equivalent to the terrestrial composition. The former ^{15}N-rich component appears to be depleted in our sample grains.

The lighter δ^{15}N value observed in some of our samples cannot be due to a fractionation process, such as Rayleigh fractionation, which would result in enrichment of heavier isotopes in nitrogen-poor fractions. Atmospheric contamination would increase nitrogen concentration (decrease 1/N), and shift the δ^{15}N value closer to zero. Hence, the variation in δ^{15}N among our samples cannot be attributed to atmospheric contamination or diffusive loss of nitrogen (Fig. 4).

Source materials and evolution history of the Ryugu parent body

Our Ryugu samples are depleted in ^{15}N compared to CI chondrites. The difference in δ^{15}N values between the bulk samples and the IOM (acid-Insoluble Organic Matter) of individual CI chondrites (*30*) suggests that nitrogen in IOM samples is also slightly ^{15}N-depleted. Furthermore, the ^{15}N-rich phase is likely to have been lost from the dehydrated CI chondrite Y-980115 through a devolatilization process. Hence, a possible carrier phase of the ^{15}N-rich end member absent to varying degrees in our samples is soluble organic/inorganic phases. The FESEM observation indicates that our Ryugu samples have CI chondrite mineralogy and lithology (Figs. 1 and S2), and hence the ^{15}N-poor material of Ryugu is different to that of Y-980115.

The measured total carbon contents are 6.8 and 6.4 wt% for the samples A0105-07 and C0106-07, respectively. The atomic C/N ratios are 112 and 88, respectively. The carbon contents are 1.5 times higher than those in CI chondrites (C/N ranging between 17 and 32: *24–28*), other Ryugu samples (*16–19*), and Y-980115 (*29*). This suggests that some decoupling between nitrogen and carbon carrier phases could have occurred. Variations observed in the δ^{15}N, and the nitrogen and carbon contents can be attributed to sample heterogeneity at a small spatial scale of samples, since the sample masses used for the measurements are between 0.12 and 0.17 mg (Table S1). The heterogeneity indicates that various carrier phases of nitrogen with distinct isotopic ratios are likely still present in other Ryugu grains. The heterogenous effects of aqueous alteration and dehydration

or devolatilization on Ryugu materials are likely to be responsible for the variation. The similarity to the dehydrated CI chondrite Y-980115 suggests that some devolatilization process may be responsible for the depletion of the ^{15}N-rich phase from our samples. This is consistent with the results of thermogravimetric analysis of a Ryugu-A sample (*16*), in which the release of interlayer water was found only above 90 °C. Such devolatilization could occur on Ryugu surface and in subsurface layers rather than in the interior of the Ryugu parent body; based on thermal modeling (*17*) the internal heating did not reach 50 °C, and hence devolatilization more likely occurred on Ryugu by some heating mechanism, such as solar radiation heating (*16*). However, the total carbon content in Y-980115 is lower than those in our Ryugu samples (*29*), which suggests that the devolatilization condition in Y-980115 is different from that in Ryugu where some enrichment in carbon relative to CI chondrites is observed. In addition to devolatilization, variable degrees of aqueous alteration may have also played a role. Most fractions of the Ryugu parent body experienced considerable aqueous alteration, but some fractions exhibit less alteration effect. This is possibly due to temperature increase at the subsurface layer of the parent body or lesser amount of water available being insufficient to drive alteration reactions (*17*). Such less altered materials are found as clasts (*17*) that might be a ^{15}N-rich carrier.

The noble gas isotopic ratios in the Ryugu samples show that Ryugu materials contain phase Q, presolar diamonds, SiC, and graphite as carriers of P1, HL, G, and R components (*21*). These are the components present in the early Solar System (*21*) prior to the formation of the parent planetesimal. The bulk Ne and Xe isotopic compositions mimic isotopic patterns seen in other CI chondrites (Fig. 3 and Table S2), supporting a genetic linkage between the noble gas carriers of the Ryugu parent body and those in CI chondrites. The elemental ratios of the heavy noble gases, ^{36}Ar, ^{84}Kr, and ^{132}Xe most resemble the P1 noble gas component (Fig. S7B). Furthermore, except for the SW-rich sample (A0105-15), the heavy noble gas concentrations are similar to those found in other CI chondrites (*31*). Some of the samples have heavy noble gas concentrations ~2–3 times higher than those in CI chondrites (Fig. 5), and are even higher than the highest concentrations observed in CM chondrites (*31–33*). In contrast to the depleted nitrogen abundances, the P1 gas in the Ryugu samples shows no evidence of being lost during potential alteration episodes. The P1 gas in the Ningqiang ungrouped C3 chondrite has been shown to be resistant to aqueous alteration (*34*), which is consistent with the high P1 abundances in the Ryugu samples. In contrast, concentrations of P1 gas in CM chondrites are correlated with their petrologic types, decreasing with higher degrees of aqueous alteration effects (*33*). Mineralogical studies suggests that the degree and condition of alteration should be different among CI, CM, and CR chondrite parent bodies (*6*). A working hypothesis is that the difference in the degree and conditions of aqueous alteration controls the P1 gas abundances. Evidently, the degree of aqueous alteration seen by the Ryugu parent body is similar to that for CI chondrites.

In addition to P1 and presolar noble gas components, Ningqiang contains another noble gas component, referred as “Ar-rich gas”, which is lost during experimental hydrothermal treatments (*34, 35*). The Ar-rich gas is also found in some less altered CR and CM chondrites (*33, 36*). These observations suggest that the carrier phase of Ar-rich gas is susceptive to aqueous alteration, and amorphous silicate is suggested to be one of its carrier phases (*35, 36*). Measurements made to date on the Ryugu samples do not show the presence of Ar-rich gas, but do indicate the presence of SW gas recently acquired during surface exposure on Ryugu. Even if the Ryugu source material contained such amorphous silicates, the Ar-rich gas could have been easily removed and lost. The absence of Ar-rich gas in the Ryugu samples is not surprising given the occurrence of the Ar-rich gas only in less altered carbonaceous chondrites.

All these lines of evidence suggest that the Ryugu's parent body formed from similar volatile components and experienced similar alteration processes to CI chondrites in the early Solar System.

Cosmic-ray produced and solar-wind derived noble gas and surface geological processes

Bulk concentrations of ^{4}He and ^{22}Ne vary significantly from 4×10^{-5} to 6×10^{-3} cm^3 STP/g, and from 3×10^{-8} to 1×10^{-5} cm^3 STP/g, respectively (Table S2), which is essentially caused by variable contributions of SW-derived gases. Based on the Ne isotopic ratios, we calculated the SW-derived ^{20}Ne and cosmogenic ^{21}Ne concentrations by subtracting contributions of the other Ne components (Table S4). The smallest cosmogenic ^{21}Ne concentration is found in a SW-^{20}Ne rich grain (A0105-15). No systematic differences in the cosmogenic ^{21}Ne concentrations are observed between the Ryugu-A and Ryugu-C samples (Fig. 6), although the higher SW-^{20}Ne concentrations were observed only in the surface samples, Ryugu-A.

The SW-^{20}Ne and cosmogenic ^{21}Ne concentrations are expected to be positively correlated as seen in regolithic meteorites (e.g., *37, 38*), if the grains have been well mixed through surface layer of the meteorites' parent bodies and experienced negligible grain-surface modification. No correlation is observed within the Ryugu samples between the SW-^{20}Ne and cosmogenic ^{21}Ne concentrations (Fig. 6). Most of the Ryugu samples plot to the lower left of the trend defined by lunar soils and regolithic meteorites (*37–41*), implying a shorter exposure history with occasional exposure to SW. We calculated SW exposure ages to be ~3500, ~250, and ~1–10 year for the A0105-15, A0105-06, and the other samples (Fig. 6), respectively. A SW-^{20}Ne flux of 4×10^{-9} cm^3 STP/cm^2/yr was calculated for the semi-major orbital axis of Ryugu (1.19 au: *42, 43*) based on the Genesis data (*44*). The sample grains are assumed to be 0.8 mm-sized (the present actual size) with a 1.8 g/cm^3 density (*17*) during SW irradiation. We assumed that the samples did not experience any grain-surface modification by pulverization or fragmentation; we regard the SW exposure ages as the lower limits.

The concentrations of cosmogenic ^{21}Ne ranges from 3×10^{-9} to 8×10^{-9} cm^3 STP/g. This excludes the SW-rich sample A0105-15, but even so this variation is somewhat smaller than those observed in the SW-^{20}Ne concentrations. We calculated the weighted means of the cosmogenic ^{21}Ne concentrations for each of the Ryugu-A and Ryugu-C samples, using the sample mass as the weighting factor. The cosmogenic ^{21}Ne concentrations are $(4.8\pm0.8)\times10^{-9}$ and $(4.3\pm0.7)\times10^{-9}$ cm^3 STP/g for the Ryugu-A and Ryugu-C samples (except for A0105-15 and C0106-01), respectively. The Ryugu-A samples are surface materials collected during the 1st touchdown sampling operation at an equatorial region by shooting a 5 g tantalum projectile at a velocity of ~300 m/s (*1, 11*), which can collect surface material (*11*). The Ryugu-C samples were recovered from a site near the artificial crater (*1*) generated during kinetic impact by the Small-Carry on Impactor (SCI: *45*). Since the depth of the artificial crater from the original surface is ~1.7m (*46*), the Ryugu-C samples may include subsurface materials as well as surface materials similar to the Ryugu-A samples. The different sampling condition between the Ryugu-A and C suggests a different history concerning SW/cosmic-ray exposure, brecciation, and meteoroid impacts. Abundances of the cosmogenic radionuclide ^{10}Be were reported to be ~12.8 and ~7.3 dpm/kg for the Ryugu-A and Ryugu-C samples, respectively (*47*), which can be explained by their different shielding depths during their residence at the surface or in the subsurface layers.

Considering the rare occurrence of a SW signature in the Ryugu samples, it is assumed that the materials recovered by the Hayabusa2 have not been transported vertically, mixed to shallower and deeper levels, by meteoroid impacts, but instead resided at a specific depth. A shielding depth

of 150 g/cm^2 is applied for the Ryugu-C samples. This corresponds to a physical depth of 1.3 m assuming a Ryugu surface layer density of 1.2 g/cm^3 density (*42*), close to the artificial crater depth of 1.7 m (*46*). The calculated production rate of ^{21}Ne (P_{21}) at 150 g/cm^2 depth is 0.79×10^{-9} cm^3 STP/g/Myr (*48*) assuming the 2π exposure at 1.19 au (*42, 43*) and CI chondrite chemistry (*49*). For the Ryugu-A samples, we assumed that the Ryugu-A samples resided at a shallow depth of 2-5 g/cm^2, not just at the surface. At this depth, cosmogenic ^{21}Ne is produced by GCRs and SCRs but SW-implanted Ne would not be a ubiquitous feature. The calculated P_{21} at this depth is 0.90×10^{-9} cm^3 STP/g/Myr. Using these production rates, we obtained cosmic ray exposure (CRE) ages of 5.3±0.9 and 5.5±0.9 Myr for the Ryugu-A and C samples, respectively. These CRE ages are averaged values of each sampling site, whereas individual grains show some variations in their cosmogenic ^{21}Ne concentrations. The variation can be explained by variable shielding depth and variation in chemistry. For the SW-rich samples A0105-15, its CRE age of more than several hundreds of kyr was obtained using a P_{21} of ~3×10^{-9} cm^3 STP/g/Myr for the depth of 0-1 g/cm^2 (*48*), where SW can be implanted at the grain surface. The CRE age of A0105-15 is longer than its SW exposure age, suggesting that the SW-rich sample was temporarily brought to the surface but was mostly buried to a deeper depth as the other samples. Because only a small fraction (~10 vol.% inferred from two SW-rich grains out of the 16 grains studied) of surface material seems to be mixed with subsurface material, a large fraction of surface layer materials down to several cm could have been liberated to interplanetary space or moved to gravitationally low-potential regions, i.e., the mid-latitude region, in ~5 Myr (the CRE ages of the samples).

Comparison with the CRE ages of meteorites is important in the interpretation of the CRE ages of Ryugu samples. Note that CRE ages for most of the meteorites would primarily reflect the duration of exposure in interplanetary space during their transit to Earth, rather than exposure on their parent bodies, as is the case for Ryugu. The cosmogenic ^{21}Ne concentrations in CI chondrites are calculated 11–25×10^{-9} (Alais), 3–6×10^{-9} (Ivuna), 6–11×10^{-9} (Orgueil), and 3×10^{-9} (Tonk) cm^3 STP/g using literature data (*14, 50*). Using the production rate of 1.5 $\times10^{-9}$ cm^3 STP/g/Myr for a 100 cm-sized body with 4π geometry (*51*), these concentrations correspond to CRE ages of 2–17 Myr. No SCR contribution and a constant GCR flux are assumed in the calculation of the production rate. Similar CRE ages for CI chondrites were obtained based on cosmogenic radionuclides (*52*), indicating that the CRE ages of CI chondrites reflect their space exposure histories, with little contribution of the parent body exposures. In the case that the parent body exposure duration are comparable to the space exposures, abundances of cosmogenic stable isotopes should be higher than those of radionuclides. Only Ivuna is thought to experience a complex exposure history (*52*). Also, it is reported that two out of the five CI chondrites have extremely short CRE ages, 0.1–0.2 Myr (*52*), and >50% of CM chondrites also have short (<10 Myr) CRE ages (*33, 53, 54*), suggesting a similar mechanism to transport CI and CM chondrite fragments into Earth-crossing orbit. Although many CM chondrites contain SW noble gases (e.g., *33*) that should be accompanied with cosmic-ray exposure on the CM parent body, the duration is not well understood. It is obvious that the Ryugu surface layer has been irradiated by SCRs and GCRs for a time duration comparable to the space exposure duration of CI, and possibly of CM chondrites. The lower collision frequency at the near-Earth orbit (*55, 56*) is responsible for the long surface residence time of Ryugu. Parent bodies of CI and CM chondrites could have experienced frequent collisions at the main belt orbit, which leads to short surface residence time on their parent bodies. Lunar surface materials likewise record a low-frequency collision history because the Moon is also a near-Earth object. The higher concentrations of SW-^{20}Ne and cosmogenic ^{21}Ne in lunar soils reflect their longer residence time, compared to those of Ryugu (Fig. 6), between surface and subsurface layers (*39–41*).

The CRE ages of the grains constrain the timing of orbital evolution of Ryugu from the main belt to the near-Earth orbit. Because the crater production rate within the asteroid belt is about 30 times higher than that in near-Earth orbits (*55, 56*), the regolith residence time in the uppermost 1 m layer on Ryugu is estimated to be 2–8 Myr for near-Earth bombardment, but for main asteroid belt bombardment it is ~0.1–0.3 Myr (*7, 8, 10*). Our noble gas study gives the surface residence time of ~5 Myr, which clearly supports the near-Earth bombardment.

After the change from main asteroid belt to near-Earth orbit, Ryugu may have experienced some surface evolution processes, in addition to meteoroid bombardment. The geographical and spectral red-blue distribution of Ryugu suggests that temporal orbital excursion near the Sun in the past may have driven reddening due to intense heating and migration of surface materials (*7, 8*). The stepped pyrolysis measurements revealed that ~30 % of cosmogenic ^{21}Ne was released at 100 °C from some samples (Fig. 3B and Table S1), indicating that the present surface and subsurface materials of Ryugu have not experienced heating above 100 °C in the past ~1 Myr. Therefore, our data support surface alteration and migration more than 1 Myr ago, rather than recent processes, being responsible for the spectral-color distribution, if the surface heating was the cause of the reddening.

The absence of a correlation between SW-^{20}Ne and cosmogenic ^{21}Ne, and the scarcity of SW in the bulk Ne isotopic ratios indicates that only a limited number of the Ryugu grains were exposed to solar wind. At this time though, it cannot be ruled out that the fraction of SW-rich grains decreased after having experienced SW exposure due to escape to space or migration from the sampling sites to other regions of Ryugu. Thermal and/or mechanical effects, such as atmospheric heating of the reentry capsule, fragmentation and pulverization in the sample catcher may also have altered the SW inventory. The CRE ages of the Ryugu grains are shorter than those of lunar soils and regolithic meteorites (*37–41*), which may also be explained by their mechanical vulnerability on Ryugu. Grain-surface modification on Ryugu is possibly related to the processes and mechanisms for the particle emissions observed on the C-type asteroid (101955) Bennu (*57*). Grain destruction by meteorite bombardment and/or phyllosilicate dehydration (*16, 57*) can be more efficient on the C-type asteroid Ryugu than on S-type asteroids.

Comparison with cosmic dust recovered on Earth

Meteoroids and micrometeorites are inevitably exposed to SW and SCRs/GCRs during their transit from their parent bodies to the Earth. Solar-wind signatures are also commonly observed in unmelted micrometeorites (UMMs) (*58–61*), most of which are similar to CI and CM chondrites in their mineralogy and chemistry. Unlike the Ryugu samples, the SW-^{20}Ne concentrations in UMMs are correlated with cosmogenic ^{21}Ne concentrations (Fig. 6). Although some fractions of the SW-^{20}Ne and cosmogenic ^{21}Ne were lost from UMMs by heating during atmospheric entry (*62*) and recoil effects (*63*), most of the UMMs contain higher amounts of SW-^{20}Ne concentrations than the Ryugu samples. This indicates that the UMMs acquired most of their SW and cosmogenic Ne not on the surface of their parent bodies but in interplanetary space, where they are always exposed to SW and cosmic rays. Unlike the UMMs, only a limited fraction of the Ryugu samples was exposed on the surface to SW, but considerable cosmogenic ^{21}Ne was produced and accumulated in the Ryugu's surface and subsurface layers. Therefore, the Ryugu surface material cannot be the major source of UMMs. Late exposure to SW in interplanetary space after liberation from Ryugu would increase abundances of SW Ne, which may explain the lower SW abundance in Ryugu material compared to those in UMMs.

Survival of pristine Ryugu material as inferred from its low-temperature released gases

Although the nitrogen compositions suggest some devolatilization effects, low temperature extraction steps (<200 °C) released 35–70 % of ^{22}Ne with isotopic ratios represented by mixing of SW and cosmogenic components (Fig. 3B and Table S2). CI chondrites also release considerable but smaller fractions of Ne below 300 °C, around 20–30 % of the total concentrations (*64*). It is possible that CI chondrites have lost some fraction of their low-temperature released noble gases during/after the fall on to Earth, whereas the Ryugu grains still retain a fraction of highly volatile noble gases acquired during the Ryugu's surface evolution. These findings imply that the Ryugu samples have not suffered from heating higher than ~100 °C since the exposure to SW and GCRs. The release temperature is consistent with abundant primordial and presolar noble gases in the Ryugu samples that are released higher temperature >900 °C (Table S2). Accordingly, Ryugu samples are the most pristine solar system materials so far. Atmospheric entry heating and/or terrestrial weathering may be responsible for the difference in the low-temperature released gases; CI chondrites have lost the most labile components during atmosphere entry, or terrestrial weathering that would produce secondary minerals and increase the retention of He and Ne in CI chondrite falls (*65*).

Conclusions

First measurements of noble gas and nitrogen isotopic compositions were performed on individual grains returned from the surface and subsurface layers of near-Earth asteroid Ryugu. The isotopic ratios of Ne and Xe are characterized by enrichments in primordial and presolar noble gases, specifically the P1 and HL components. These isotopic compositions and their concentrations are similar to those in CI chondrites, indicating a genetic relationship between the Ryugu source materials and CI chondrites. Nitrogen isotopes exhibit marked difference from CI chondrites: Part of the samples are depleted in nitrogen, and show lower δ^{15}N values. The noble gas and nitrogen isotope features suggest that Ryugu contains various and abundant carrier phases that have not lost their volatiles and are not mixed with each other. Thus, Ryugu contains pristine volatile carriers that could be one of the major sources of the Earth's volatiles.

Records of SW, GCR, and SCR irradiations after the formation of Ryugu were deciphered from the He and Ne isotopic compositions. The CRE ages of ~5 Myr for the grains are compatible with regolith residence time estimated for near-Earth bombardment, indicating that Ryugu left the main belt orbit several Myr ago. The current surface and subsurface materials on Ryugu have not experienced heating above 100 °C within the last ~1 Myr.

This study, combined with companion papers of other Ryugu sample analyses and remote-sensing approaches, suggests that the volatile compounds originally incorporated in the primitive bodies were continuously processed during the asteroid evolution processes. The pristine volatile carriers in Ryugu offer clues to uncovering the evolution of solar system volatiles.

References and Notes

1. Y. Tsuda et al., Hayabusa2 mission status: Landing, roving and cratering on asteroid Ryugu. *Acta Astronaut.* **171**, 42–54 (2020).
2. S. Watanabe et al., Hayabusa2 Mission Overview. *Space Sci. Rev.* **208**, 3–16 (2017).
3. B. Marty, The origins and concentrations of water, carbon, nitrogen and noble gases on Earth. *Earth. Planet. Sci. Lett.* **313–314**, 56–66 (2012).
4. M. W. Broadley et al., Identification of chondritic krypton and xenon in Yellowstone gases and the timing of terrestrial volatile accretion. *Proc. Natl. Acad. Sci.* 117, 13997–14004 (2020).

5. G.R. Huss, A.E. Rubin, J.N. Grossman, "Thermal metamorphism in chondrites" in *Meteorites and the Early Solar System II* (University of Arizona Press, 2006) pp. 567–586.
6. A. Brearley, The action of water. *Meteorites and the Early Solar System II*, D. S. Lauretta and H. Y. McSween Jr. (eds.), University of Arizona Press, Tucson, 943 pp., p.584-624 (2006)
7. S. Sugita et al., The geomorphology, color, and thermal properties of Ryugu: Implications for parent-body processes. *Science* **364**, eaaw0422 (2019).
8. T. Morota et al., Sample collection from asteroid (162173) Ryugu by Hayabusa2: Implications for surface evolution. *Science* **368**, 654–659 (2020).
9. Y. Cho et al., Geologic history and crater morphology of Asteroid (162173) Ryugu. *J. Geophy. Res.: Planets* **126**, e06572 (2021).
10. N. Takaki et al., Resurfacing processes constrained by crater distribution on Ryugu. *Icarus* 377, 114911 (2022)
11. S. Tachibana et al., Pebbles and sand on asteroid (162173) Ryugu: in situ observation and particles returned to Earth. *Science* **375**, 1011-1016 (2022).
12. T. Yada et al., Ryugu: Preliminary analysis of the Hayabusa2 samples returned from C-type asteroid Ryugu. *Nature Astronomy* **6**, 214–220 (2022).
13. Materials and methods are available as supplementary materials.
14. A. J. King et al., The Yamato-type (CY) carbonaceous chondrite group: Analogues for the surface of asteroid Ryugu? *Geochemistry* **79**, 125531 (2019).
15. G. Matrajt et al., FTIR and Raman analyses of the Tagish Lake meteorite: Relationship with the aliphatic hydrocarbons observed in the Diffuse Interstellar Medium. *Astronomy Astrophys.* **416**, 983-990 (2004).
16. T. Yokoyama et al., Chemical characterization of asteroid Ryugu samples. *Science,* this issue (2022).
17. T. Nakamura et al., Formation and evolution of Cb-type asteroid Ryugu: direct evidence from returned samples. *Science,* this issue (2022).
18. H. Yabuta et al., Macromolecular organic materials recording aqueous activity on parent body of the asteroid Ryugu. *Science,* this issue (2022).
19. H. Naraoka et al., Organic compounds from Ryugu – Prebiotic molecules in a C-type asteroid. *Science,* this issue (2022).
20. H. Busemann, H. Baur, R. Wieler, Primordial noble gases in "phase Q" in carbonaceous and ordinary chondrites studied by closed-system stepped etching. *Meteorit. Planet. Sci.* **35**, 949–973 (2000).
21. U. Ott. Planetary and pre-solar noble gases in meteorites. *Chemie der Erde* **74**, 519–544 (2014).
22. V.S. Heber et al., Noble gas composition of the solar wind as collected by the Genesis mission. *Geochim. Cosmochim. Acta* **73**, 7414–7432 (2009).
23. A. Grimberg et al., Solar wind neon from Genesis: Implications for the lunar noble gas record. *Science* **314**, 1133–1135 (2006).
24. C. -C. Kung, R.N. Clayton, Nitrogen abundances and isotopic compositions in stony meteorites. *Earth Planet. Sci.* **38**, 421–435 (1978).
25. F. Robert, S. Epstein, The concentration and isotopic composition of hydrogen, carbon and nitrogen in carbonaceous meteorites. *Geochim. Cosmochim. Acta* **46**, 81–95 (1982).
26. J.F. Kerridge, Carbon, hydrogen and nitrogen in carbonaceous chondrites: Abundances and isotopic compositions in bulk samples. *Geochim. Cosmochim. Acta* **49**, 1707–1714 (1985).
27. V.K. Pearson, M.A. Sephton, I.A. Franchi, J.M. Gibson, I. Gilmour, Carbon and nitrogen in carbonaceous chondrites: Elemental abundances and stable isotopic composition. *Meteorit. Planet. Sci.* **41**, 1899–1918 (2006).

28. C.M.O'D. Alexander et al., The Provenances of asteroids, and their contributions to the volatile inventories of the terrestrial planets. *Science* **337**, 721–723 (2012).
29. Q.H.S. Chan, Y. Chikaraishi, Y. Takano, N. Ogawa, N. Ohkouchi, Amino acid compositions in heated carbonaceous chondrites and their compound-specific nitrogen isotopic ratios. *Earth Planet. Space* **68**, article id. 7 (2016).
30. C.M.O'D. Alexander, M. Fogel, H. Yabuta, G.D. Cody, The origin and evolution of chondrites recorded in the elemental and isotopic compositions of their macromolecular organic matter. *Geochim. Cosmochim. Acta* **71**, 4380–4403 (2007).
31. E. Mazor, D. Heymann, E. Anders, Noble gases in carbonaceous chondrites. *Geochim. Cosmochim. Acta* **34**, 781–824 (1970).
32. C.A. Goodrich et al., The first samples from Almahata Sitta showing contacts between ureilitic and chondritic lithologies: Implications for the structure and composition of asteroid 2008 TC_3. *Meteorit. Planet. Sci.* **54**, 2769–2813 (2019).
33. D. Krietsch et al., Noble gases in CM carbonaceous chondrites: Effect of parent body aqueous and thermal alteration and cosmic ray exposure ages. *Geochim. Cosmochim. Acta* **310**, 240–280 (2021).
34. Y. Yamamoto, R. Okazaki, T. Nakamura, Effects of experimental aqueous alteration on the abundances of argon-rich noble gases in the Ningqiang carbonaceous chondrite. *Meteorit. Planet. Sci.* **41**, 541–551 (2006).
35. T. Nakamura, M. Zolensky, M. Sekiya, R. Okazaki, K. Nagao, Acid-susceptive material as a host phase of argon-rich noble gas in the carbonaceous chondrite Ningqiang. *Meteorit. Planet. Sci.* **38**, 243–250 (2003).
36. T. Obase et al., Water-susceptible primordial noble gas components in less-altered CR chondrites: A possible link to cometary materials. *Geochim. Cosmochim. Acta* **312**, 75–105 (2021).
37. R. Wieler, H. Baur, A. Pedroni, P. Signer, P. Pellas, Exposure history of the regolithic chondrite Fayetteville: I. Solar-gas-rich matrix. *Geochim. Cosmochim. Acta* **53**, 1441–1448 (1989).
38. T. E. Ferko et al., The irradiation history of the Ghubara (L5) regolith breccia. *Meteorit. Planet. Sci.* **37**, 311–327 (2002).
39. J. K. Agrawal, K. Gopalan, M. N. Rao, Solar wind and cosmogenic rare gases in Luna 16 and 20 soils and their correlation with cosmic ray produced fossil tracks in lunar samples. *Pramana* **3**, 176-185 (1974).
40. J. L. Jordan, D. Heymann, S. Lakatos, Inert gas patterns in the regolith at the Apollo 15 landing site. *Geochim. Cosmochim. Acta.* **38**, 65-78 (1974).
41. N. B. Bhai, K. Gopalan, J.N. Goswami, M.N. Rao, T.R.Venkatesan, Solar cosmic ray produced neon and xenon isotopes and particle tracks in feldspars from lunar fines 14148 and 24087. *Proc. Lunar Planet. Sci. Conf.* **9th**, 1627–1645 (1978).
42. S. Watanabe et al., Hayabusa2 arrives at the carbonaceous asteroid 162173 Ryugu—a spinning top-shaped rubble pile. *Science* **364**, 268–272 (2019).
43. S. Kikuchi et al., Hayabusa2 pinpoint touchdown near the artificial crater on Ryugu: Trajectory design and guidance performance. *Adv. Space Res.* **68**, 3093–3140 (2021).
44. A. Grimberg, H. Baur, F. Bühler, P. Bochsler, R. Wieler, Solar wind helium, neon, and argon isotopic and elemental composition: Data from the metallic glass flown on NASA's Genesis mission. *Geochim. Cosmochim. Acta* **72**, 626–645 (2008).
45. T. Saiki et al., Small carry-on impactor of Hayabusa2 mission. *Acta Astronautica* **84**, 227–236 (2013).

46. M. Arakawa et al., An artificial impact on the asteroid (162173) Ryugu formed a crater in the gravity-dominated regime. *Science* **368**, 67–71 (2020).
47. K. Nishiizumi et al., Exposure conditions of samples collected on Ryugu's two touchdown sites determined by cosmogenic nuclides. *Hayabusa Symposium 2021*, S3-1 (2021).
48. C.M. Hohenberg, P.K. Davis, W.A. Kaiser, R.S. Lewis, J.H. Reynolds, Comparisons between observed and predicted cosmogenic noble gases in lunar samples. *Proc. Lunar Planet. Sci. Conf.* **9th**, 2311–2344 (1978).
49. K. Lodders, B. Fegley, *The planetary scientist's companion.* (*New York: Oxford University Press*, 1998).
50. L. Schultz, L. Franke, Helium, neon, and argon in meteorites: A data collection. *Meteorit. Planet. Sci.* **39**, 1889–1890 (2004).
51. I. Leya, J. Masarik, Cosmogenic nuclides in stony meteorites revisited. *Meteorit. Planet. Sci.* **48**, 1061–1086 (2002).
52. K. Nishiizumi, M.W. Caffee, Exposure histories of CI1 and CM1 carbonaceous chondrites. *Lunar Planet. Sci. Conf.* **43rd**, #2758 (2012).
53. G.F. Herzog, M.W. Caffee, "Cosmic-ray exposure ages of meteorites" in *Treatise on Geochemistry* (Elsevier, ed. 2, 2014) pp. 419-453.
54. E.R.D. Scott, G.F. Herzog, Short cosmic-ray exposure ages of CI and CM Chondrites may reflect disintegration of volatile-rich asteroids at perihelion *Lunar Planet. Sci. Conf.* **52nd**, #1833 (2021).
55. W. F. Bottke Jr. et al., Linking the collisional history of the main asteroid belt to its dynamical excitation and depletion. *Icarus* **1**, 63–94 (2005).
56. D. P. O'Brien, R. Greenberg, The collisional and dynamical evolution of the main-belt and NEA size distributions. *Icarus* **178**, 179–212 (2005).
57. D. S. Lauretta et al., Episodes of particle ejection from the surface of the active asteroid (101955) Bennu. *Science* **366**, eaay3544 (2019).
58. T. Osawa, K. Nagao, Noble gas compositions of Antarctic micrometeorites collected at the Dome Fuji Station in 1996 and 1997. *Meteorit. Planet. Sci.* **37**, 911–936 (2002).
59. T. Osawa, T. Nakamura, K. Nagao, Noble gas isotopes and mineral assemblages of Antarctic micrometeorites collected at the meteorite ice field around the Yamato Mountains. *Meteorit. Planet. Sci.* **38**, 1627–1640 (2003).
60. K. Bajo et al. Single grain noble gas analysis of Antarctic micrometeorites by stepwise heating method with a newly constructed miniature furnace. *Earth Planet. Space* **63**, 1097–1111 (2011).
61. R. Okazaki et al. Mineralogy and noble gas isotopes of micrometeorites collected from Antarctic snow. *Earth. Planet. Space* **67**, 90 (2015).
62. E. Füri, A. Aléon-Toppani, B. Marty, G. Libourel, Effects of atmospheric entry heating on the noble gas and nitrogen content of micrometeorites. *Earth Planet. Sci. Lett.* **377–378**, 1–12 (2013).
63. R. Trappitsch, I. Leya, Cosmogenic production rates and recoil loss effects in micrometeorites and interplanetary dust particles. *Meteorit. Planet. Sci.* **48**, 195–210 (2013).
64. D.C. Black, On the origins of trapped helium, neon and argon isotopic variations in meteorites-II. Carbonaceous meteorites. *Geochim. Cosmochim. Acta* **36**, 377–394 (1972).
65. A. J. King, K.J.H. Phillips, S. Strekopytov, C. Vita-Finzi, S.S. Russell, Terrestrial modification of the Ivuna meteorite and are assessment of the chemical composition of the CI type specimen. *Geochim. Cosmochim. Acta* **268**, 73–89 (2020).
66. R.C. Reedy, Solar-proton production of neon and argon. *Proc. Lunar Planet. Sci. Conf.* **23rd**, 1133–1134 (1992).

67. J. F. Ziegler, *Nucl. Instrum. Methods Phys. Res. B* **219-220**, 1027–1036 (2004).
68. M. Honda et al., Redetermination of the ^{21}Ne relative abundance of the atmosphere, using a high resolution, multi-collector noble gas mass spectrometer (HELIX-MC Plus). *Inter. J. Mass Spectrom.* **387**, DOI:10.1016/j.ijms.2015.05.012 (2015).

SOM References:

69. H. Sawada et al. Hayabusa2 sampler: Collection of asteroidal surface material. *Space Sci. Rev.* **208**, 81–106 (2017).
70. B. Harbecke, Application of Fourier's allied integrals to the Kramers-Kronig transformation of reflectance data. *Appl. Phys.* **A40**, 151–158 (1986).
71. M. K. Weisberg, M. Prinz, R.N. Clayton, T.K. Mayeda, The CR (Renazzo-type) carbonaceous chondrite group and its implications. *Geochim Cosmochim. Acta* **57**, 1567–1586 (1993).
72. A. Brearley, Phyllosilicates in the matrix of the unique carbonaceous chondrite, LEW 85332 and possible implications for the aqueous alteration of CI chondrites. *Meteoritics Planet. Sci.* **32,** 377–388 (1997).
73. M. Zolensky, R. Barrett, L. Browning, Mineralogy and composition of matrix and chondrule rims in carbonaceous chondrites. *Geochim Cosmochim. Acta* **57**, 3123-3148 (1993).
74. R. Okazaki, K. Nagao, Primordial and cosmogenic noble gases in the Sutter's Mill CM chondrite. *Meteorit. Planet. Sci.* **52**, 669–689 (2017).
75. A. Ishida A., K. Hashizume, T. Kakegawa, Microbial nitrogen cycle enhanced by continental input recorded in the Gunflint Formation. *Geochem. Perspect. Lett.* **4**, 13–18 (2017).
76. J. D. Gilmour, I. C. Lyon, W. A. Johnston, G. Turner, Relax - an ultrasensitive, resonance ionization mass-spectrometer for xenon. *Rev. Sci. Instrum.* **65**, 617–625 (1994).
77. S. A. Crowther et al., Characteristics and applications of RELAX, an ultrasensitive resonance ionization mass spectrometer for xenon. *J. Anal. At. Spectrom.* **23(7),** 938–947 (2008).
78. T. Lawton, On the xenology of comets and other primitive reservoirs in the solar system. PhD Thesis, The University of Manchester (2021).
79. P.R. Heck et al., Lifetimes of interstellar dust from cosmic ray exposure ages of presolar silicon carbide. *Proc Natl Acad Sci U S A* **117**, 1884–1889 (2020).
80. H. Baur, "Numerische Simulation und praktische Erprobung einer rotationssymmetrischen Ionenquelle für Gasmassenspektrometer," thesis, ETH Zurich, Zurich, Switzerland (1980).
81. M. E. I. Riebe et al., Cosmic-ray exposure ages of six chondritic Almahata Sitta fragments. *Meteorit. Planet. Sci.* **52**, 2353–2374 (2017).
82. K. Kitazato et al., The surface composition of asteroid 162173 Ryugu from Hayabusa2 near-infrared spectroscopy. *Science* **364**, 272–275 (2019).
83. D. Takir, K.R. Stockstill-Cahill, C.A. Hibbitts, Y. Nakauchi, 3-µm reflectance spectroscopy of carbonaceous chondrites under asteroid-like conditions. *Icarus* **333**, 243–251 (2019).
84. H.C. Bates, K.L. Donaldson, A.J. King, N.E. Bowles, S.S. Russell, A spectral investigation of aqueously and thermally altered CM, CM-an, and CY chondrites under simulated asteroid conditions for comparison with OSIRIS-REx and Hayabusa2 observations. *JGR Planets* **126**, https://doi.org/10.1029/2021JE006827 (2021).
85. M. Matsuoka et al., Spectral and mineralogical alteration process of naturally-heated CM and CY chondrites. *Geochim. Cosmochim. Acta* **316**, 150–167 (2022).
86. S. Potin et al., Style and intensity of hydration among C-complex asteroids: A comparison to desiccated carbonaceous chondrites. *Icarus* 346, 113826 (2020).
87. F.A. Miller, C.H. Wilkins, Infrared spectra and characteristic frequencies of inorganic ions. *Anal. Chem.* **24**, 1253–1294 (1952).

88. M. Ozima, F.A. Podosek, *Noble Gas Geochemistry* (Cambridge Univ. Press, ed. 2, 2002).

Acknowledgments:

We thank the anonymous reviewers and the editors for their helpful comments and suggestions. Hayabusa2 was developed by JAXA, in collaboration with the German Aerospace Center, the Centre National d'Études Spatiales, NASA, and other universities, institutes, and companies in Japan. The sampler system was developed by JAXA, The University of Tokyo, Hokkaido University, Kyushu University, Japan Agency for Marine-Earth Science and Technology, and other universities, institutes, and companies in Japan. **Funding:** RO was supported by JSPS KAKENHI (grant JP19H01959, JP20H05846). BM, EF, MWB and DB were supported by the European Research Council (PHOTONIS Advanced Grant # 695618 and VOLATILIS Starting Grant 715028) and by the Centre National d'Etudes Spatiales (CNES). Work by D.K., M.R. and H.B. has been carried out within the framework of the NCCR Planets and the Ambizione program supported by the Swiss NSF (grants 200020_182649, 51NF40-182901, PZ00P2_193331). JG, SC, TL and LF were funded by STFC grants numbers ST/R000751/1 and ST/V000675/1. PLC was supported by UKRI FLF grant number MR/S03465X/1. KH and AI were supported by JSPS KAKENHI Grant Number JP20H00190. **Author contributions:** RO led the sample preparation and NG-MS analysis at Kyushu U. with YM and wrote the paper with contributions from members of the Hayabusa2-initial-analysis volatile team. Hayabusa2 capsule recovery and curation works: led by HS, ST, YNM, KS, TY, and RO. FESEM analysis at JAXA: led by TY. FTIR spectroscopy at JAXA: led by FK. Nitrogen and NG-MS at CRPG-Nancy: led by MWB, BM, DB, and EF. Xe-MS analysis at Manchester: led by JG, TL, SC and LF. NG-MS analysis at Washington U.: led by AM and OP. NG-MS analysis at ETH: performed by HB, DK, CM and MR. Nitrogen&NG-MS analysis at Ibaraki U.: led by KH and AI. All authors discussed the results and commented on the manuscript. **Competing interests:** The authors declare no competing interests. **Data and materials availability:** All images used in this study and the TRIM simulation result are available at the JAXA Data Archives and Transmission System (DARTS) at https://data.darts.isas.jaxa.jp/pub/hayabusa2/paper/Okazaki_2022a. Data of Hayabusa2 samples and other data from the mission are available at https://www.darts.isas.jaxa.jp/curation/hayabusa2 and https://www.darts.isas.jaxa.jp/planet/project/hayabusa2/, respectively. The samples of Ryugu are curated by the JAXA Astromaterials Science Research Group; distribution for analysis is through an Announcement of Opportunity available at https://jaxaryugu-sample-ao.net. Our samples studied are listed in Table S1.

Supplementary Materials

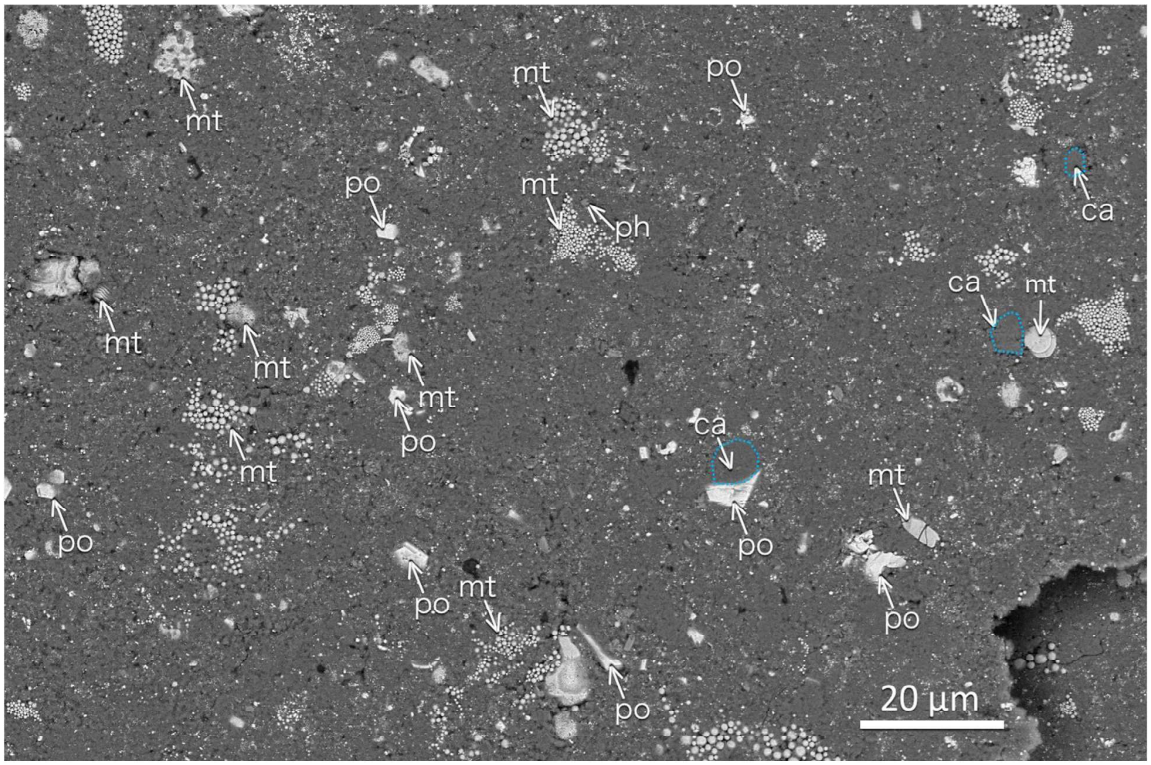

Fig. 1. Back scattered electron image of a Ryugu pellet sample (A0105-10). The sample is mainly composed of phyllosilicates. Framboidal and plaquette magnetites and sulfides are also ubiquitously present. Carbonates tend to coexist with magnetites and sulfides. "mt" stands for magnetite, "po" for pyrrhotite, iron sulfide, "ca" for carbonate, and "ph" for Ca-phosphate, respectively.

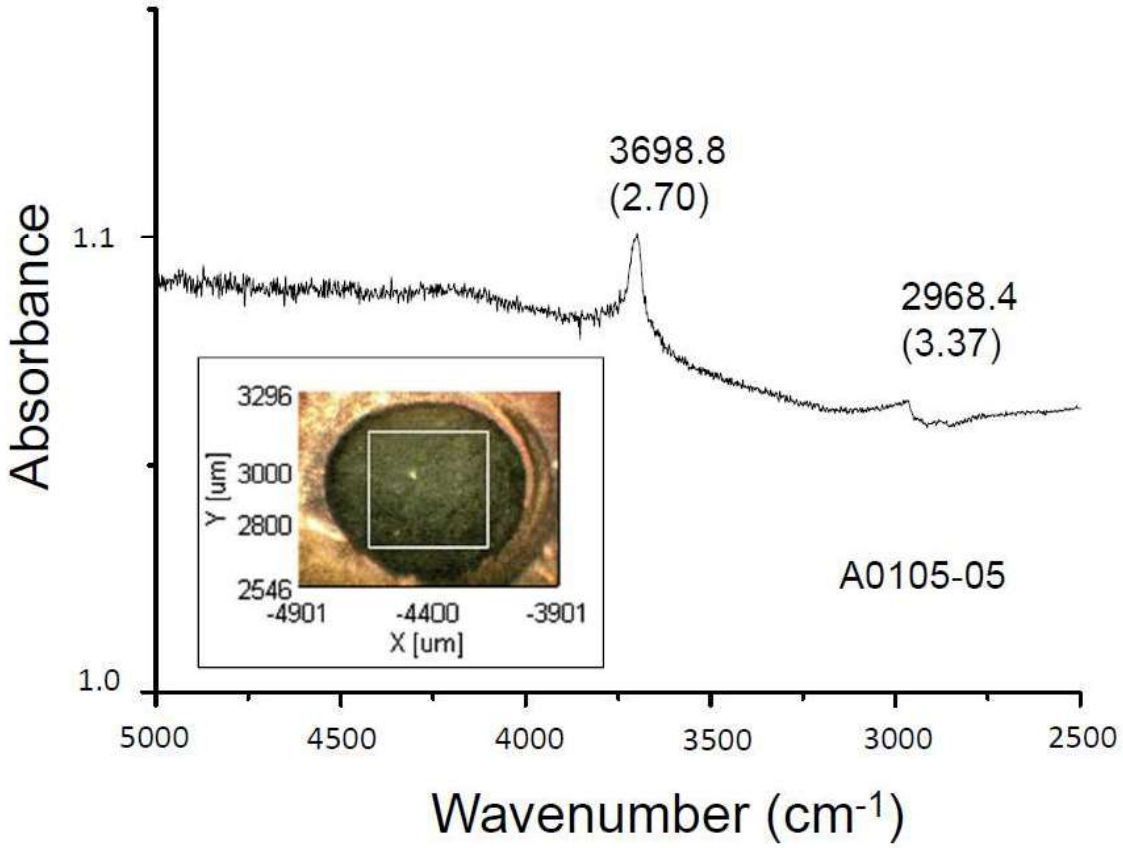

Fig. 2. A typical IR spectrum of a Ryugu pelletized sample (A0105-05). The O-H stretching of phyllosilicates at 3698.8 cm^{-1} (2.70 μm) was commonly observed in all samples. The aliphatic C-H stretching at 2968.4 cm^{-1} (3.37 μm) was also observed in almost all samples. The white square in the image indicates the analyzed area (aperture size 450 × 450 $μm^2$).

5

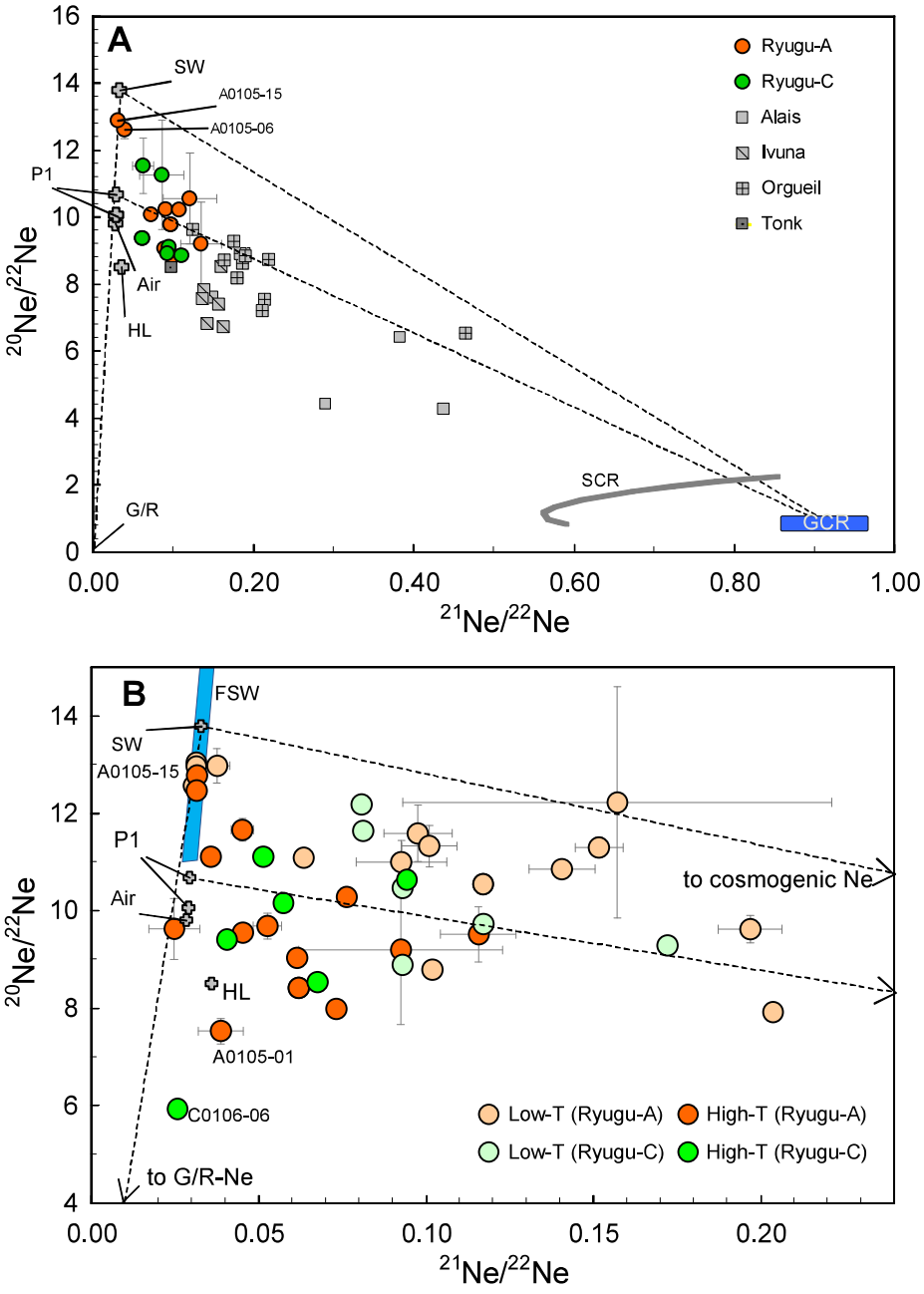

Fig. 3. Isotopic ratios of Ne in the Ryugu samples. Most bulk Ne isotope data (Fig. 3A) are consistent with mixing of P1, HL, and cosmogenic Ne, though some samples clearly require a contribution from solar wind (SW) Ne. Low-T data (for 50–200 °C fractions or the first laser extraction steps) indicate a contribution from SW in all samples whereas High-T data (for >900 °C fractions or the later laser extraction steps) exhibit contributions from P1 or HL, and G-Ne in two cases (Fig. 3B). Compositions of galactic- (GCR) and solar-cosmic ray (SCR) produced Ne (for an exponential rigidity shape of 100 MeV: *66*), and fractionated SW (FSW: *23*, calculated

using TRIM simulation [*67*] for the CI chemistry and the depth between 20 and 100 nm [*13*]) are shown. Error bars are 1σ. Data sources: *14*, *20–22*, *50*, *66*, *68*.

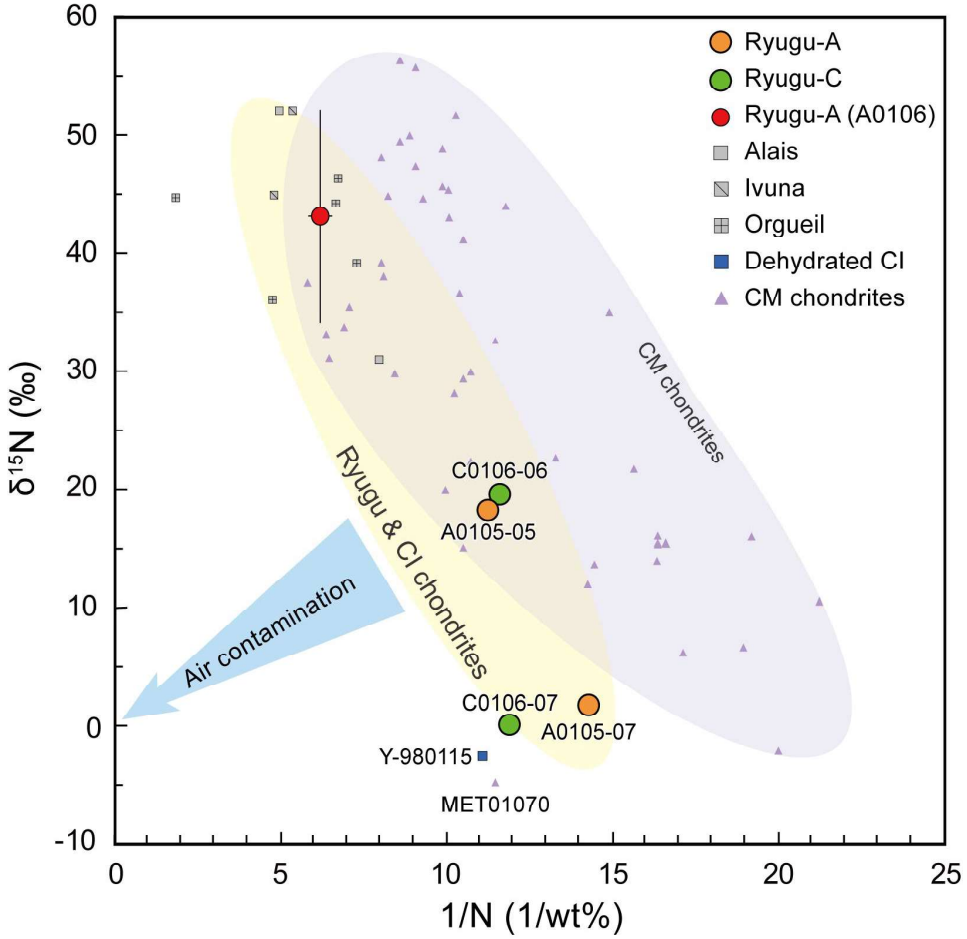

Fig. 4. Nitrogen isotopic compositions and inverse of nitrogen concentrations of the Ryugu pellet samples determined by stepped combustion analysis. The bulk $\delta^{15}N$ values of A0105-07 and C0106-07 are ~0 and ~+20 ‰, lower than those of CI chondrites (*28*), but plot close to the dehydrated CI-like chondrite Y-980115 (*29*) and the highly altered CM1 chondrite MET01070 (*28*). The other two samples (A0105-05 and C0106-06) plot intermediate between A0105-07/C0106-07 and CI chondrite compositions. Uncertainties (1σ) for our data are smaller than the symbols' size. Data sources: *19*, *24–29*.

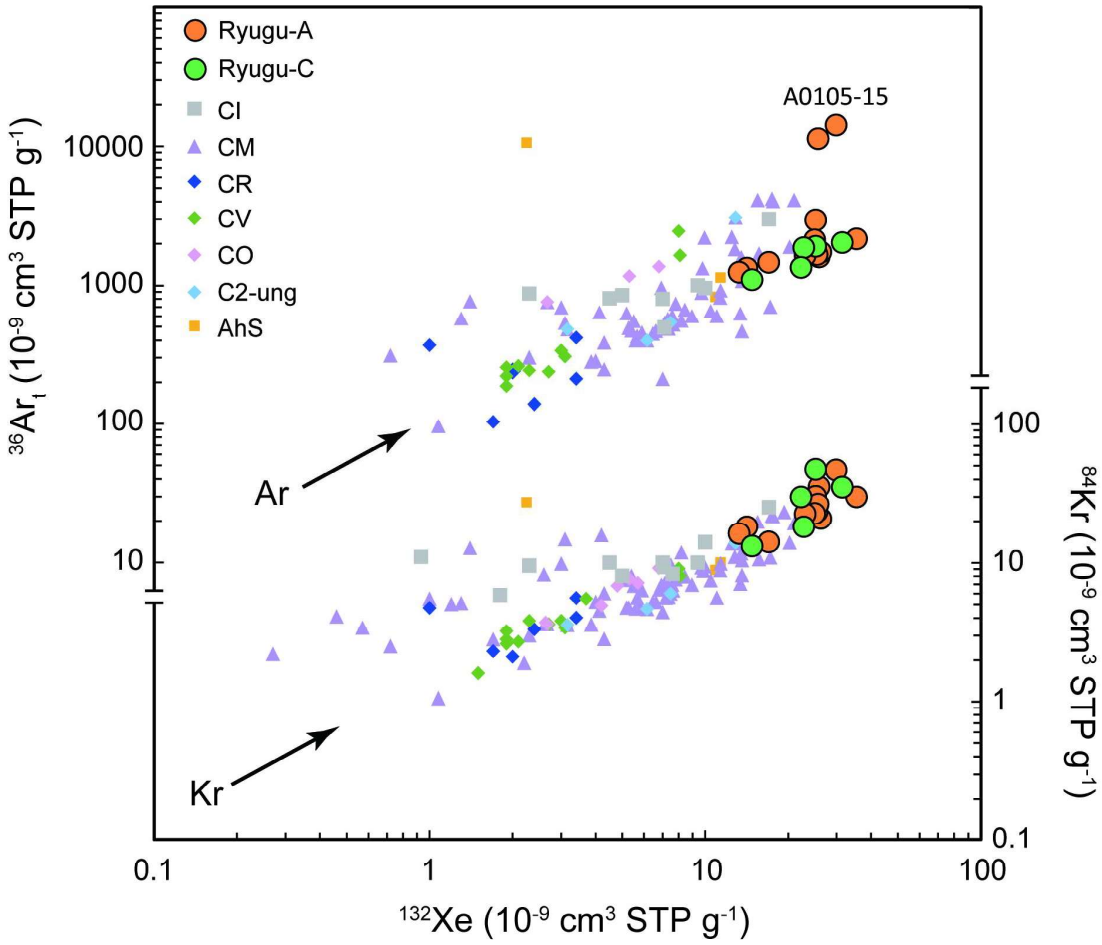

Fig. 5. Concentrations of heavy noble gases. The Ryugu grains contain higher concentrations of primordial noble gases compared to any other chondrites, including CI chondrites. C2-ung denotes ungrouped C2 chondrites. AhS denotes a carbonaceous-chondrite-like clast from the Almahata Sitta polymict ureilite (*32*). Uncertainties (1σ) are 10%. Data sources: *31–33*.

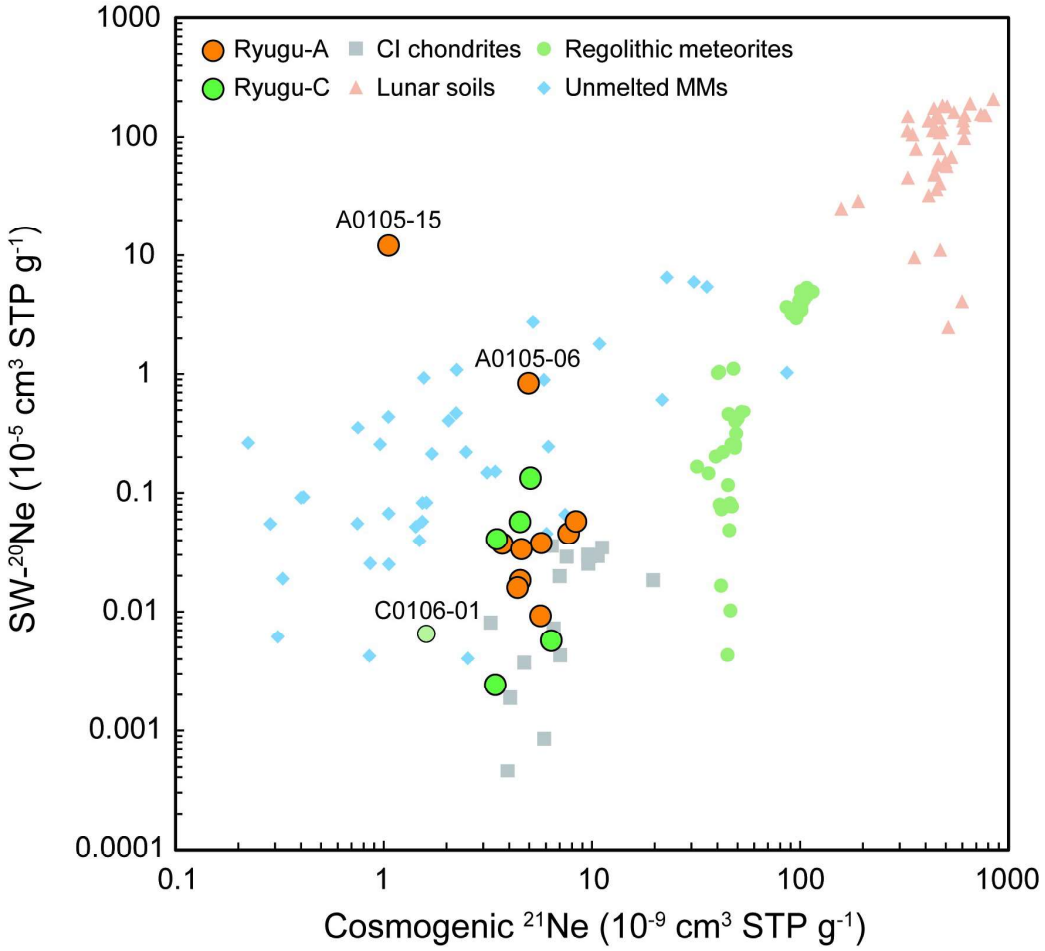

Fig. 6. Bulk concentrations of solar wind (SW) origin ^{20}Ne and cosmogenic ^{21}Ne. Two Ryugu samples (A0105-06 and -15) show clear excess in SW-^{20}Ne. No positive correlation between the SW-^{20}Ne and cosmogenic ^{21}Ne was found. The concentrations in C0106-01 are preliminary (Table S4). Uncertainties (1σ) are 10%. Data sources: *37–41, 58–61*.

Science
AAAS

Supplementary Materials for

Noble gases and nitrogen in Ryugu grains – Records of its past and recent geological activity

Ryuji Okazaki[1*], Bernard Marty[2], Henner Busemann[3], Ko Hashizume[4], Jamie D. Gilmour[5], Alex Meshik[6], Toru Yada[7], Fumio Kitajima[1], Michael W. Broadley[2], David Byrne[2], Evelyn Füri[2], My E.I. Riebe[3], Daniela Krietsch[3], Colin Maden[3], Akizumi Ishida[8], Patricia Clay[5], Sarah A. Crowther[5], Lydia Fawcett[5], Thomas Lawton[5], Olga Pravdivtseva[6], Yayoi N. Miura[9], Jisun Park[10,11], Ken-ichi Bajo[12], Yoshinori Takano[13], Keita Yamada[14], Shinsuke Kawagucci[15,16], Yohei Matsui[15,16], Mizuki Yamamoto[1], Kevin Righter[17], Saburo Sakai[13], Naoyoshi Iwata[18], Naoki Shirai[19,20], Shun Sekimoto[21], Makoto Inagaki[21], Mitsuru Ebihara[22], Reika Yokochi[23], Kunihiko Nishiizumi[24], Keisuke Nagao[25], Jong Ik Lee[25], Akihiro Kano[26], Marc W. Caffee[27,28], Ryu Uemura[29], Tomoki Nakamura[8], Hiroshi Naraoka[1], Takaaki Noguchi[30,31], Hikaru Yabuta[32], Hisayoshi Yurimoto[12], Shogo Tachibana[33], Hirotaka Sawada[7], Kanako Sakamoto[7], Masanao Abe[7], Masahiko Arakawa[34], Atsushi Fujii[7], Masahiko Hayakawa[7], Naoyuki Hirata[34], Naru Hirata[35], Rie Honda[36], Chikatoshi Honda[35], Satoshi Hosoda[7], Yu-ichi Iijima[7†], Hitoshi Ikeda[7], Masateru Ishiguro[37], Yoshiaki Ishihara[38], Takahiro Iwata[7], Kosuke Kawahara[7], Shota Kikuchi[39], Kohei Kitazato[35], Koji Matsumoto[40,41], Moe Matsuoka[42], Tatsuhiro Michikami[43], Yuya Mimasu[7], Akira Miura[7], Tomokatsu Morota[26], Satoru Nakazawa[7], Noriyuki Namiki[40,41], Hirotomo Noda[40,41], Rina Noguchi[44], Naoko Ogawa[7], Kazunori Ogawa[7], Tatsuaki Okada[7], Chisato Okamoto[34†], Go Ono[7], Masanobu Ozaki[7,41], Takanao Saiki[7], Naoya Sakatani[45], Hiroki Senshu[39], Yuri Shimaki[7], Kei Shirai[7,34], Seiji Sugita[26], Yuto Takei[7], Hiroshi Takeuchi[7], Satoshi Tanaka[7], Eri Tatsumi[26,46], Fuyuto Terui[47], Ryudo Tsukizaki[7], Koji Wada[39], Manabu Yamada[39], Tetsuya Yamada[7], Yukio Yamamoto[7], Hajime Yano[7], Yasuhiro Yokota[7], Keisuke Yoshihara[7], Makoto Yoshikawa[7], Kent Yoshikawa[7], Shizuho Furuya[7], Kentaro Hatakeda[48], Tasuku Hayashi[7], Yuya Hitomi[48], Kazuya Kumagai[48], Akiko Miyazaki[7], Aiko Nakato[7], Masahiro Nishimura[7], Hiromichi Soejima[48], Ayako Iwamae[48], Daiki Yamamoto[7,49], Kasumi Yogata[7], Miwa Yoshitake[7], Ryota Fukai[7], Tomohiro Usui[7], Harold C. Connolly Jr.[50], Dante Lauretta[51], Sei-ichiro Watanabe[29], and Yuichi Tsuda[7].

Correspondence to: okazaki.ryuji.703@m.kyushu-u.ac.jp

This PDF file includes:

Tables S1 to S4

Materials and Methods

Sample preparation and analysis flow

The Hayabusa2 sample catcher/container was brought back to the JAXA curation facility after the recovery operation in Woomera, South Australia (*11*). The Ryugu samples were collected and treated within a vacuum chamber and ultra-pure nitrogen chambers (*12*). Eight milligrams of the Ryugu grains were allocated to the volatile sub-team and used for chemical analysis of volatile components, along with infrared spectroscopic and electron-microprobe observations.

The Ryugu grains allocated to the volatile sub-team are ~1 mm-sized grains in diameter. Twenty-two grains (~4 mg total weight) were picked up from the chamber A (samples #A0105-01 – A0105-22), in which the surface materials of Ryugu sampled from the first touchdown site were stored. Twelve grains (samples #C0106-01 – C0106-12: Table S1), including one large grain (2.5 mm in size), were collected from the sapphire dish of the chamber C (*12*), in which samples were stored from the second touchdown site after the Small Carry-on Impactor (SCI: *45*) operation (*1, 46*) that made an artificial crater on and excavated sub-surface materials from Ryugu. Hayabusa2 sampled solid asteroidal materials by two methods; by kicking up material with a tantalum projectile (~5g) with 300 m s^{-1} injection velocity, and by hooking and lifting up it with a bent tip of the sampler horn (*11, 69*). The allocated Ryugu grains were transferred to Kyushu U. from the JAXA, and were pelletized to obtain flat surfaces for the surface analyses. Pelletization operation might change the microstructure of hydrous minerals, but leaves those of magnetites (framboidal) and pyrrhotite (platy) (Fig. 1). The force employed for pelletizing (0.6 N with a 4 mm screw) is too small to change the volatile compositions, which is confirmed by the presence of low-temperature released gases from Ryugu samples and by the rehearsal analysis of the Murchison pellet sample. Details about the method of the pelletization will be presented elsewhere (in preparation).

Individual pelletized samples (samples #A0105-01 to -16, and C0106-01 to -08: Table S1) were analyzed by FT-IR and FESEM installed at the JAXA curation facility. After the examinations/analyses, the pellet samples were distributed to each laboratory of the volatile sub-team in order to carry out noble gas, nitrogen, and other light element analyses (Fig. S1). Preliminary results of cosmogenic nuclide measurements coupled with noble gas analysis were reported by (*52*). The full data and discussion will be presented elsewhere.

Fourier-Transform Infrared Spectroscopy

Fourier-Transform infrared (FT-IR) spectra were obtained using a JASCO IRT-5000 spectrometer with a mercury-cadmium-telluride (MCT) detector at JAXA/ISAS. The microscope uses a Schwarzschild-Cassegrain objective (×16). Pelletized samples were mounted in a viewport equipped with a CaF_2 window developed for this analysis to eliminate the exposure of the samples to terrestrial atmosphere. The spectrometer was housed inside an acryl box with continuous nitrogen flow. Mid-IR reflectance spectra (5000–600 cm^{-1}) of the bulk samples were obtained under the following conditions: A total of 256 scans of spectra at 2 cm^{-1} spectral resolution were accumulated. The aperture sizes for bulk analyses were chosen in order to cover the sample surfaces as widely as possible, for A0105-01 ～ 16; 400×400 (-01,-06,-09), 380×380 (-02), 450×450 (-03,-05,-07,-08,-12), 360×380 (-04), 280×430 (-10), 500×380 (-11), 500×500 (-13,-16), 450×400 (-14), 400×320 (-15) μm^2, for C-0106-01 ～ 08; 350×350 (-01), 400×400 (-02,-05,-07,-08), 500×500 (-03), 300×500 (-04), 450×450 (-06) µm2. Mapping analyses were also carried out under the following conditions: Aperture size was 75×75 μm^2 for each section and a

total of 64 scans of spectra were accumulated for each section. The results of the mapping analyses will be discussed in elsewhere.

In the region from 2000 to 600 cm^{-1}, in particular, the peaks of the spectra were distorted to look like those of a first derivative curve, therefore the Kramers-Kronig relation was used to transform them into ordinary spectra (e.g., *70*). The vertical axis *K* in S5 represents the extinction coefficient of complex index of refraction.

Scanning electron microscopy

Each of the pelletized samples was analyzed using a Hitachi Schottky field emission scanning electron microscope (FE-SEM) SU6600 equipped with an energy-dispersive X-ray spectrometer (EDS) Oxford Instruments X-MAX150 in the Extraterrestrial Sample Curation Center (ESCuC) of JAXA. The FE-SEM has a custom equipped air lock that can be evacuated and purged with nitrogen gas in which one can set and remove a cap of a seal-type sample holder. Utilizing this system, all the samples were analyzed without exposure to air. The pelletized samples were analyzed in low vacuum mode (~60 Pa) without any conductive coating, with 9 kV in acceleration voltage and 0.2 nA in beam current. In order to avoid possible contamination and damage by electron beam irradiation, we only performed point analyses and avoided map analyses. Figure S2 shows backscattered electron (BSE) images of some of the pelletized samples. The grains are pressed into a holder made of copper to be flat and smoothed on their surfaces. As mentioned in the main text, they are mainly composed of matrices (shown gray in the images) containing ubiquitously distributed Fe-sulfides and magnetites (showing white inclusions). Four to six representative areas were selected from each of the samples for point analyses to identify chemical compositions of phases and minerals. Several square areas of the matrix of 5 to 10 μm in size were analyzed in each area for analyses of matrices. Figure S3 shows a (Si+Al)-Mg-Fe ternary plot for analyzed matrices in the pelletized samples of A0105 and C0106. The saponite and serpentine solid solution lines, as well data from analyses of matrices of CI, CM and CR chondrites, are indicated in the plot (*71, 72*). The compositions of the pelletized samples are mostly distributed between the saponite and serpentine line, although a certain amount of them are plotted toward Fe-enriched and Mg-enriched compositions over the serpentine line. Those of Fe-enriched composition are likely due to presences of Fe sulfides, magnetites and serpentine-tochilinite intergrowth phases (*73*) at sub-micron scales. Those of Mg-enriched could be due to sub-micron carbonates such as dolomites in the analyzed area. Although compositional data in this study may be more qualitative than quantitative (EDS compared to wave dispersive spectrometer, WDS), the chemical composition of matrices of Ryugu samples studied here are comparable to CI chondrites, which would be consistent with the previous reports and companion papers (*12, 16, 17*).

Noble gas and nitrogen analyses

Noble gas isotopes were measured at five laboratories, Kyushu U., Ibaraki U., CRPG-Nancy, ETH, U. of Manchester, and Washington U. Nitrogen isotopes were measured at Ibaraki U. and CRPG-Nancy.

At Kyushu U.:

Noble gases were extracted by using an infrared lamp and a small-sized furnace, called Pot-pie furnace (*74*). The Ryugu samples wrapped in Al foils were installed at the sample holder attached to the Pot-pie furnace, and heated at 50 °C *in vacuo* for 11 hours prior to the

measurements. The IR lamp was used to heat the samples at 100 and 200 °C, while the higher temperature extractions were performed with the Potpie furnace. Evolved gases were purified with Ti-Zr getters and an Al/Zr getter (NP 10: SAES®). The noble gases were separately introduced to a modified MM-5400 mass spectrometer using charcoal traps. Blank levels by using the IR lamp were 3×10^{-12}, 1×10^{-13}, 1×10^{-10}, 2×10^{-14}, and 2×10^{-15} cm^3STP (Standard Temperature (0 °C) and Pressure (1 bar)) for ^{4}He, ^{20}Ne, ^{40}Ar, ^{84}Kr, and ^{132}Xe, respectively. Blank gases of the Pot-pie were 2×10^{-11}, 8×10^{-13}, 4×10^{-10}, 5×10^{-14}, and 1×10^{-14} cm^3STP for ^{4}He, ^{20}Ne, ^{40}Ar, ^{84}Kr, and ^{132}Xe, respectively. Details about the NG-MS at Kyushu U. are given in (*74*).

At CRPG-Nancy:
Noble gases and nitrogen were extracted from grains A0105-05 and C0106-06 by CO_2 laser heating and analyzed using Helix MC+ (Thermo Scientific) and Noblesse HR (Nu Instruments) noble gas mass spectrometers respectively. He-Ne-Ar-Kr-Xe-N_2 abundances and isotope ratios were determined for two laser heating extraction steps of grain A0105-05 using the Helix MC+ mass spec. After laser heating, ~10% of the extracted gas was isolated in a glass cold finger for nitrogen analysis, while the rest was exposed to series of hot Ti-sponge getters for purification. Noble gases were separated using a stainless steel cryogenic trap and a charcoal cold finger held at -196°C, and were introduced sequentially into the Helix MC+ for analysis. The remaining aliquot was introduced into a quartz-glass line and purified for N_2 analysis using a CuO furnace cycled between 450°C and 950°C, and two cold fingers held at -180°C, before being introduced into the Helix MC+. Procedural blanks were 9.45×10^{-11} cm^3 STP for ^{4}He, 2.40×10^{-12} cm^3 STP for ^{20}Ne, 8.83×10^{-13} cm^3 STP for ^{36}Ar, 1.3×10^{-14} cm^3 STP for ^{84}Kr, 3.8×10^{-15} cm^3 STP for ^{130}Xe, and 6.3×10^{-8} cm^3 STP for $^{28}N_2$. Ne-Ar-N_2 abundances and isotope ratios of grain C0106-06 were determined sequentially on the Noblesse HR at a trap current of 150 µA. Noble gases were purified using two hot (600 °C) Ti sponge getters and two cold (room temperature) SAES™ Ti-Al getters. Argon was separated from neon by adsorption onto a charcoal finger at -196 °C. Nitrogen was purified in a Pyrex and quartz-glass line using a CuO furnace cycled between 723 and 1173 K and a U-shaped cold trap held at 93 K. Procedural blanks for the Noblesse line were 1.28×10^{-7} cm^3 STP for $^{28}N_2$, 3.20×10^{-12} cm^3 STP for ^{20}Ne, and 7.17×10^{-11} cm^3 STP for ^{40}Ar.

At Ibaraki U.:
The solid sample wrapped in a platinum foil was installed in a branch of a furnace made of a double-walled quartz tube. During the baking of the quartz tube at 1000 °C under the vacuum, the sample at the branch was heated at around 50 °C by the radiation. After the preheating of the sample, the sample dropped into the quartz tube was heated at designated temperatures in approximately 1 Torr pure oxygen, by the stepwise combustion method. The bulk sample results reported in this paper represent the totals of 15 or 17-step analyses performed using this method. During the combustion, the extracted gas was in contact with a platinum foil heated at 800 °C. The condensable gases were removed by a cryogenic trap. After absorbing the remaining oxygen gas by CuO, a fraction of the gas that mainly consist of nitrogen and noble gases was put into contact with a Ti-Zr getter before argon isotope measurement. Another fraction of the gas, after pressure adjustment, was finally introduced to the mass-spectrometer operating in static-mode for nitrogen mass-spectrometry. (See *75* and references therein for further procedural details and analytical performances.) Standard gas measurements were performed 21 times in total during

the analytical session of the two Hayabusa2 solid samples. The reproducibility for the nitrogen isotope ratio during this session was 0.7 ‰ (1σ) for 60 picomole standard N_2 gases. System blank levels of nitrogen vary by the combustion temperature, but are as low as 1 picomole at 800 ^{o}C when approximately 80 % of the nitrogen gas was extracted from the samples. Carbon concentrations were determined from the CO_2 pressure evolved during the combustion. CO_2 along with other gases including H_2O and SO_2 were first trapped by the cryogenic trap cooled at liquid nitrogen temperature. After absorption of the oxygen gas by CuO, only CO_2 were then liberated from the trap maintained at a temperature for ice-liquid mixture of isopropyl alcohol. The CO_2 pressure measurement were done using a crystal pressure gauge calibrated using the CO_2 gas generated from weighted amounts of pure-carbon.

At U. Manchester:
Xenon isotopic compositions were analyzed using the RELAX mass spectrometer (*76, 77*). Three sapphire dishes containing fragments produced during the production of pellets were loaded into the laser port of the spectrometer and baked (< 150 °C) prior to analysis. Gas was extracted from the samples using an infrared Fiber Laser (JK Lasers, JK50FL, λ = 1080 nm) with a spot size large enough to cover all material visible in the dishes. Two samples (A0105-03 and A010512) were heated at low temperature to remove any surface adsorbed gases, and at high temperature to attempt to fully degas the particles in a single heating step. The high temperature step was repeated while moving the position of the dish relative to the laser to ensure all material had been heated and fully degassed. The third sample (C0106-02) was step-heated in roughly equal temperature increments to see if it was possible to separate different xenon components.

Each aliquot was purified by exposure to a getter (Zr–V–Fe alloy SAES®), then the xenon was condensed on a cold spot (~80 K) within the ion source of the mass spectrometer. After 45 s the spectrometer was isolated and the cold sport warmed by pulsed heating laser (λ = 1064 nm) to desorb the condensed gases. Analysis then proceeded as discussed in *77 and 78*.

Sample gas heating steps were punctuated by procedural blanks (~3300 atoms or ~1.2×10^{-16} cm^3STP ^{132}Xe) and measurement of an air standard (1.2×10^5 atoms or ~4.5×10^{-15} cm^3STP ^{132}Xe). Air standards allow absolute quantities of gas to be calculated, and for a correction to be made for instrument dependent mass fractionation. The data we present are corrected and calibrated accordingly.
The material in the sapphire dishes was too small to weigh using the balances available. Sample mases were estimated from images taken using an optical microscope prior to analysis. ImageJ was used to estimate the areas of individual grains, the grains were assumed to be spherical, and a density of 1.8 gcm^{-3} (*17*) adopted to estimate masses.

At ETH:
The three samples (two Ryugu pellets, A0105-02 and C0106-01, and a Murchison pellet allocated for rehearsal purposes) were wrapped in Pt foil, weighed, and loaded into the laser sample chamber all in a nitrogen atmosphere. The PE glove bag was purged and refilled three times from a 5N nitrogen supply before each use. We determined masses of 0.0632±0.0004 mg and 0.1589±0.0010 mg for the Murchison sample and A0105-02, respectively. For sample C0106-01, we encountered a mass deficit likely caused by a loss of Pt foil during the loading process (we found remnants of metal in the loading device). We assigned a nominal mass of 0.100 mg for this sample. Small fragments of C0106-01 were produced in the pelletization process, once analyzed, the concentrations of noble gases in these will provide us with further

constraints on the mass of pellet C0106-01. Once attached to the extraction line, we pre-heated the samples to ~110 °C in ultra-high vacuum for several days prior to analysis. During analysis, gases were released by heating with an Nd:YAG infrared laser (λ=1064 nm, ~60 µm laser spot) for 2 min at 66 % output power (100 % = 16 W; e.g. *79*). These conditions are sufficient to degas the sample material, while the Pt remains essentially unaffected. We measured re-extractions ("step-2"; Table S2) for all samples at 68 % laser power for 2 min. The re-extractions yielded negligible gas amounts for all samples in all elements, except for Ar, Kr, and Xe in Ryugu sample A0105-02 (Table S2). For this sample, we measured, thus, an additional re-extraction ("step-3") at 69 % laser power for 2 min to confirm full gas extraction. Prior to the measurement, the gases were purified using a cold trap (kept at ~−50 °C) and successively in a series of SAES getters and separated into three fractions (He-Ne, Ar, Kr-Xe) by freezing at different temperatures. Typically, we measured 13 % of the total Ar in the Kr-Xe fraction and 8 % and 2 % of the total Kr and Xe, respectively, in the Ar fraction, which was corrected for. The three noble gas fractions were sequentially analyzed using the ETH Zurich inhouse-built static-vacuum sector-field noble gas mass spectrometer "Albatros" that is equipped with a Baur-Signer ion source (*80*). For details on the instrument and the measurement procedure (see, e.g., *81*). Several calibration measurements using noble gas standards with known amounts and compositions were performed to determine the mass discrimination and sensitivity of the instrument. Blanks were measured by heating empty Pt foil packages following the same procedure as the sample measurements. Typical blank corrections amounted to <0.4 % for He, <2.3 % for ^{36,38}Ar, <59 % for ^{40}Ar, <6.4 % for Kr, and <2.9 % for Xe. The Ne blank was unsatisfactorily high (~15.8×10^{-12} cm^{3}STP for ^{20}Ne, resulting in ~40 % correction) when measuring Murchison and Ryugu sample C0106-01. We identified the cover glass, installed within the sample chamber on top of the sample holder to protect the laser viewport, as the source of the high Ne blank. The cover glass was removed before measuring Ryugu sample A0105-02. This significantly reduced the Ne blank (~0.9×10^{-12} cm^{3}STP for ^{20}Ne) resulting in Ne blank corrections <2.8 % for this sample.

At Washington U.
High sensitivity (5 mA/Torr at 0.25 mA electron emission) 21 cm radius 90° magnetic sectors mass-spectrometer was used for these analyses. This, built in-house, instrument is equipped with > 90 % ion transmission ion source without e-focusing magnet (*80*). It operates at 3 kV acceleration voltage for Kr, Xe and Ar and at 4 kV for light noble gases. This configuration results in low memory and long (> 1 hour for Xe and Kr) useful ion-counting time. Instrumental mass discrimination is extremely small (~0.06 %/u for Xe) and stable due to the absence of magnetic field in the ion source region. Gas was extracted in miniature oven separated from all-metal (except for 1" dia, ¼" thick sapphire view port for pyrometery) sample loading device. Chemically active gases were removed using a series of SEAS getters and freshly deposited Ti-films. Hot tungsten filament facilitated cracking of complex hydrocarbons into fragments that are more readily react with getter material. Noble gases were separated cryogenically before the isotopic analyses. Typical Xe blank (1770 °C × 10 min) was ~3×10^{-15} cm^{3}STP. It was determined by melting Pt foil having the same weight as the Pt capsules containing samples A0105-04(P) and C0106-05(P).

Calculation method of TRIM simulation

The isotopic composition of implantation-fractionated solar wind (FSW: *23*) was calculated using TRIM simulation (*67*). The condition of the TRIM calculation is as follows: Implantation isotopes are ^{3}He, ^{4}He, ^{20}Ne, ^{21}Ne, and ^{22}Ne. Their speed of the isotopes is 446.0 km/s, corresponding to 3.109, 4.126, 20.608, 21.641, 22.669 keV for kinetic energies of ^{3}He^{+}, ^{4}He^{+}, ^{20}Ne^{+}, ^{21}Ne^{+}, and ^{22}Ne^{+}, respectively. No variation in the energies was considered. The total number of these ions is 1×10^{5}. The chemical composition of the target material is assumed to be that of the CI chondrite average (*49*) regarding H, C, N, O, Na, Mg, Al, Si, S, Ca, Cr, Mn, Fe, and Ni. The incidence angle between the ions and the target is 0˚.

Supplementary Text

Electron microprobe observations and infrared spectroscopy of the Ryugu samples

The FESEM observation shows that the Ryugu grains are mainly composed of fine-grained matrices, in which phyllosilicates occur as the major mineral phase (Fig. 1 and S2). Chondrules and refractory inclusions (Ca-Al-rich inclusion, CAI) were not observed so far. Magnetites, sulfides, carbonates, and Ca-phosphates are ubiquitously distributed throughout the matrices (Fig. 1). Modal abundances of magnetite and Fe sulfides were estimated based on the BSE images (Fig. S2) by decreasing the color depths to 7 gray levels and counting the number of pixels of each color. Although this estimation has an uncertainty larger than those obtained by EDS mapping, it is possible to distinguish whether the modal abundances of these minerals in the Ryugu samples are similar to those in CI chondrites or not. The abundances of magnetites and sulfides in Ryugu-A are 5±2 and 2±1 % (n=16), respectively, while those in Ryugu-C are 5±2 and 3±2 % (n=8), with no systematic differences between Chamber-A and C samples. These abundances are similar to those in CI chondrites, clearly different from those in CM and dehydrated CI-like carbonaceous chondrites (*14*). The Energy-dispersive X-ray spectroscopy (EDS) data shows that the chemical compositions of the matrices and typical minerals are similar/identical to those of the CI chondrite matrices (*13* and Fig. S3).

The FT-IR spectrum of A0105-05, obtained for an area of 450 x 450 μm^{2}, is typical of the allocated samples (Fig. 2). In the region of 5000–2500 cm^{-1} (Fig. 2), O-H stretching of phyllosilicates (*15*) at 3698.8 cm^{-1} (2.70 μm) and C-H stretching (*15*) at 2968.4 cm^{-1} (3.37 μm) are observed, which is essentially consistent with the results reported for the bulk Ryugu samples (*e.g., 12*). The position of O-H stretching from phyllosilicates is at slightly shorter wavelength compared with the value (2.72 μm) of the previous remote-sensing report (*82*). That position closely resembles that of CI chondrites centered at ~2.71 μm due to Mg-serpentine and clay minerals than that of CM chondrites centered at ~2.80 μm likely due to the presence of Fe-serpentine - cronstedtite (*83*). Also, the position of the 2.71 μm feature of our samples is different from those of heated CM and CY chondrites (~2.9 μm after heating at 150 °C: *84*, and ~2.80 μm after 400 °C heating: *85*). The differences in the 2.71 μm feature may be attributed partly to adsorbed water on these meteorites (*86, 87*). The 3.1 μm feature (e.g., *12*) was not observed in our Ryugu samples, which may be due to the insufficient sensitivity of the spectrometer.

Calculation of the cosmogenic ^{21}Ne and trapped Ne abundances

Isotopic ratios of Ne in the Ryugu samples can be explained by mixing of P1, HL, SW, G/R, and cosmogenic Ne (Fig. 3 and Table S2). We calculated the abundances of each

component in the samples by assuming that each extraction step contained cosmogenic, SW, and one trapped Ne component. A different trapped Ne component is assumed for different extraction steps and samples. Because in most of the cases, it is difficult to identify the most likely trapped component, we applied two models with a different trapped component (*Table S4*). Trapped components are selected not to obtain negative cosmogenic ^{21}Ne concentrations, considering that the Orgueil CI chondrite contains HL and P1 Ne components as the main components (*21*). Model 1 considers the release temperature of the components (e.g., lower temperature of HL compared to that of P1 component) and hence is more preferable case than Model 2.

Air contamination effects on noble gas isotopic compositions of the Ryugu samples

Similar to the light noble gases, considerable fractions of heavy noble gases were released at lower temperature (<200 °C), up to ~30% (*Table S2*). The elemental ratios of the 200 °C fractions of the fragmental samples (treated under atmospheric environment) of A0105-06(F) and C0106-04(F) are enriched in ^{84}Kr compared to those of P1 gas (Fig. S7B), suggesting a contribution of elementally fractionated Earth's atmosphere. Three pelletized samples of A0105-10(P), -15(P) and C0106-08(P) also show the enrichment of ^{84}Kr. Contribution of Earth's atmosphere can be seen in the step-heating Xe data for A0105-10(P), -10(F), -11(F), -15(F), and C0106-08(P). The contribution from atmospheric gases are not common in the pelletized samples, indicating that the contamination could have happened during operations handling each sample, i.e., during and/or after the pelletization, and that the Ryugu samples were not initially contaminated by Earth's atmosphere.

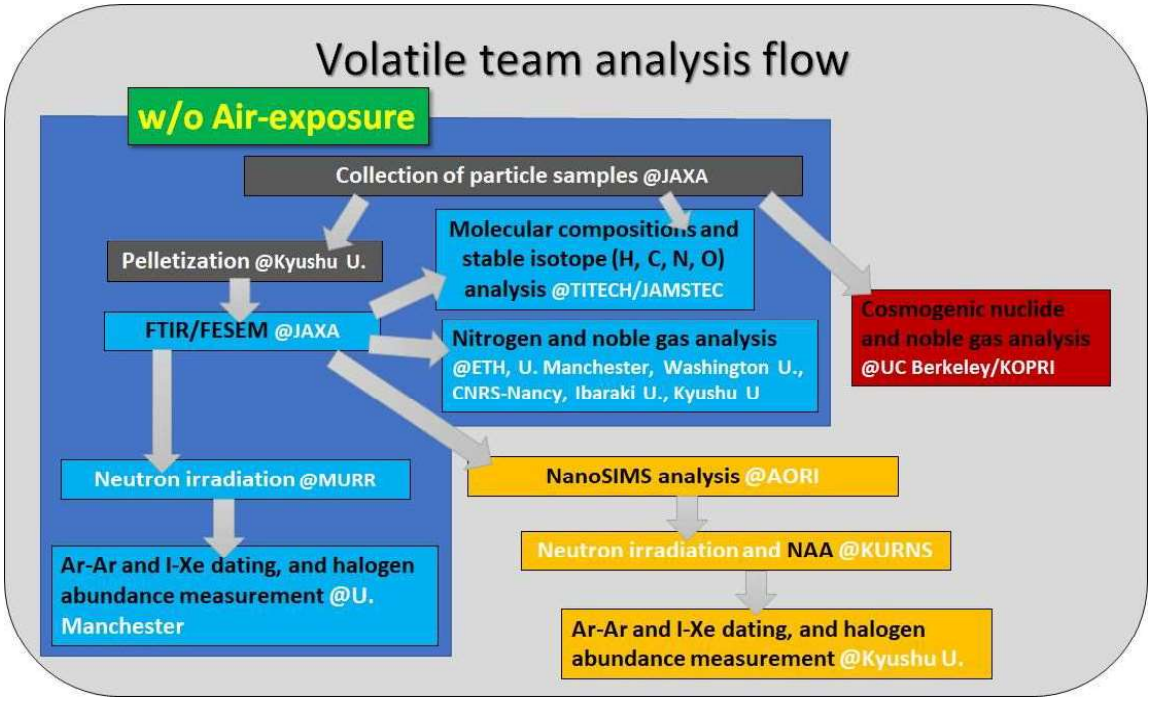

Fig. S1. Analytical flow of the volatile team of the Hayabusa2 initial analysis. Our analytical plan consists of three approaches; 1) native volatiles and I-Xe/halogen analyses by using samples that were treated WITHOUT air-exposure throughout the whole process (blue boxes), 2) combined analyses between NanoSIMS, neutron activation analysis (NAA), and Ar-Ar dating (orange boxes), 3) cosmogenic long-lived nuclides and noble gas isotopes (red box).

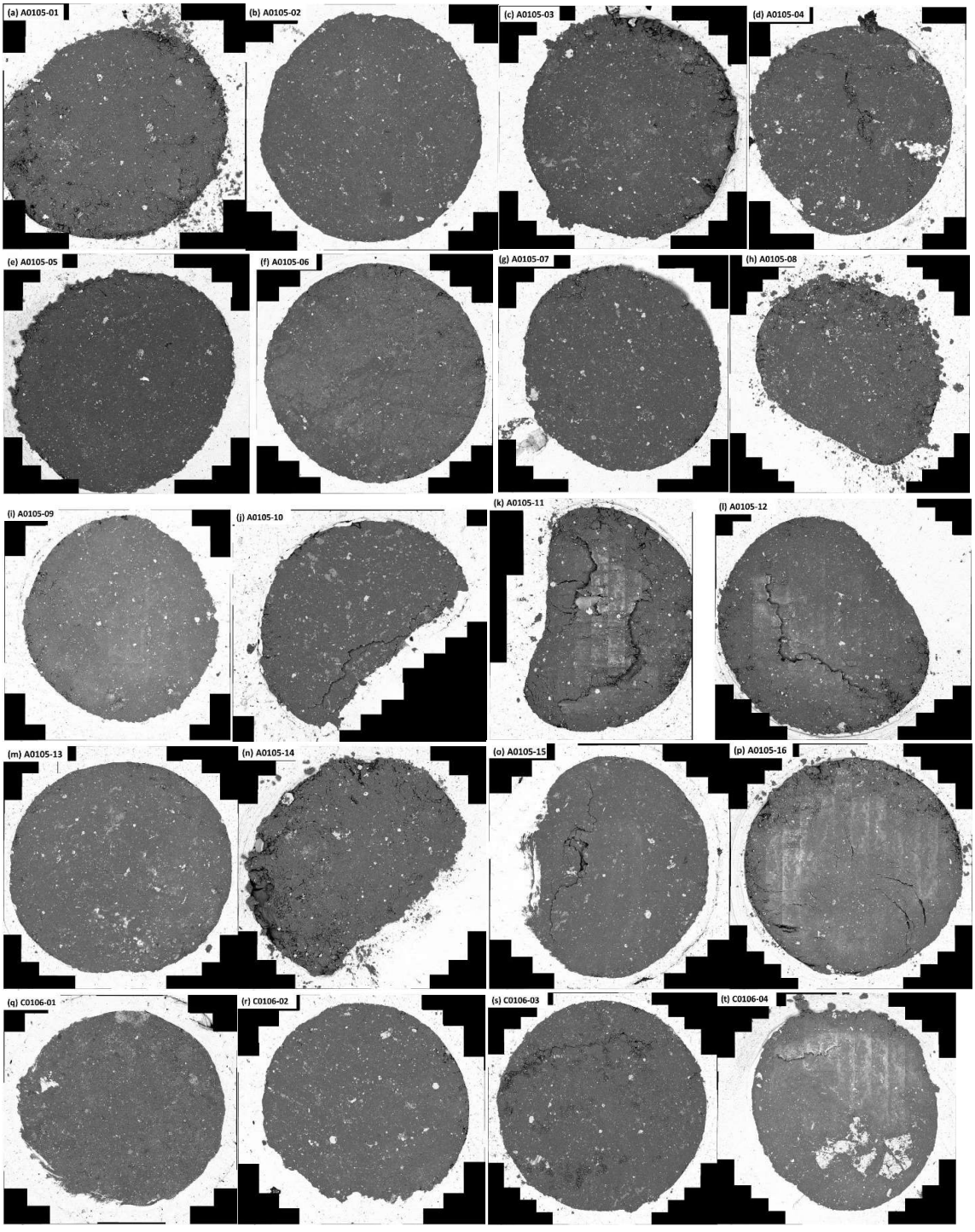
(a) A0105-01
(b) A0105-02
(c) A0105-03
(d) A0105-04
(e) A0105-05
(f) A0105-06
(g) A0105-07
(h) A0105-08
(i) A0105-09
(j) A0105-10
(k) A0105-11
(l) A0105-12
(m) A0105-13
(n) A0105-14
(o) A0105-15
(p) A0105-16
(q) C0106-01
(r) C0106-02
(s) C0106-03
(t) C0106-04

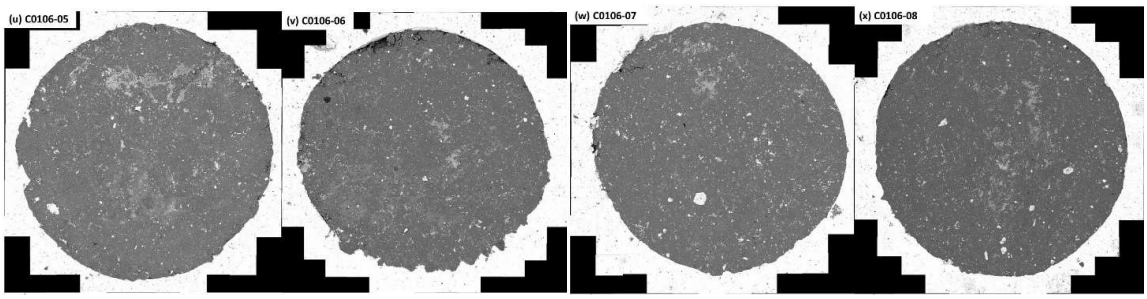

Fig. S2. Backscattered electron images of pelletized Ryugu samples. The width of each image is ~1 mm. (a)-(p) are A0105 particles obtained from Chamber A, first touchdown samples and (q)-(x) are C0106 particles from Chamber C, the second touchdown samples. There is no significant difference between those from Chamber A and C. They are mostly composed of matrices (gray) with ubiquitously distributed magnetites (most of the bright spots/minerals) and sulfides (the brightest spots/minerals). A0105-04 and C0106-04 contain large magnetites and Fe sulfides. The surrounding bright area is the sample holder made of cupper, in which each sample grain was mounted during the pelletization procedure.

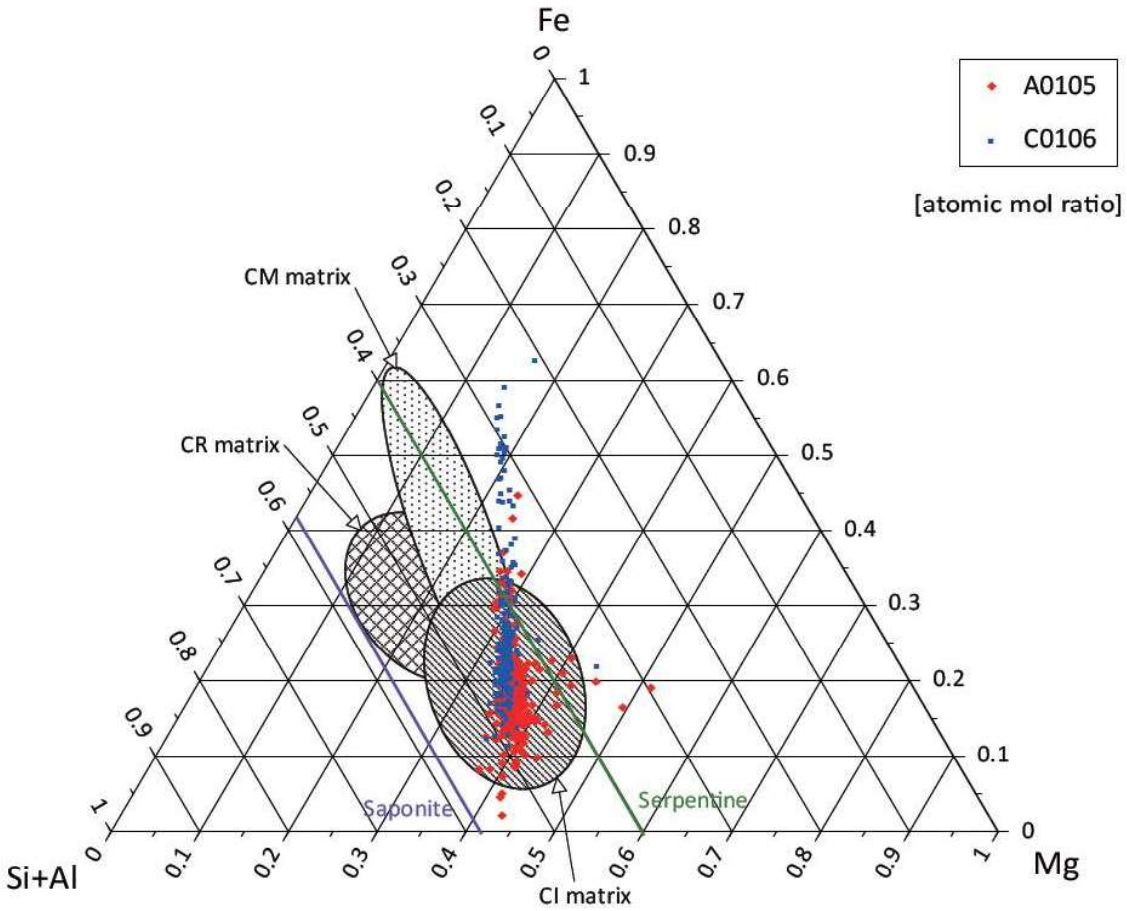

Fig. S3. A Si+Al-Mg-Fe ternary diagram of chemical compositions of matrix areas of A0105 and C0106 (atomic mol ratio). For references, saponite and serpentine solid solution lines as well as chemical compositions of CI, CM and CR chondrites are also displayed (*72, 73*). Ryugu matrix areas plot mostly in the CI region, although some are plotted toward Fe-enriched or Mg-enriched compositions.

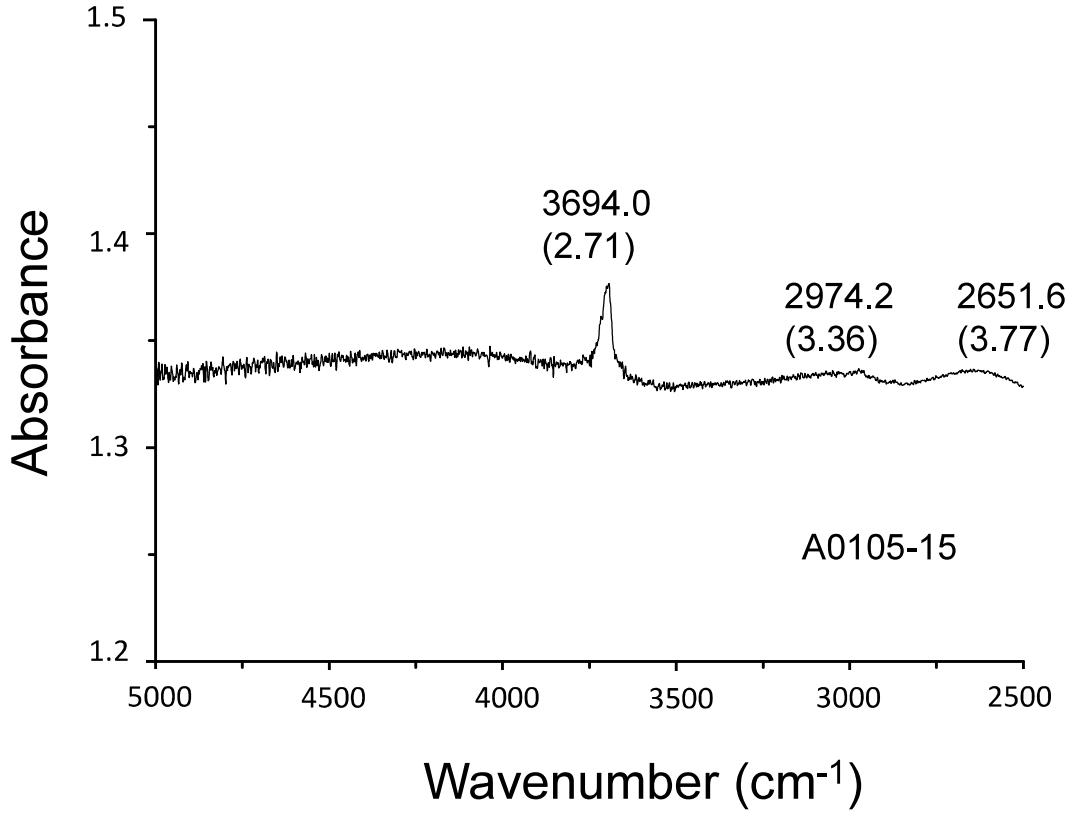

Fig. S4. FT-IR spectrum for A0105-15. A notable broad absorption around 2651.6 cm^{-1} (3.77 μm) was observed only in A0105-15, in which the highest concentrations of SW-derived He and Ne amongst the samples were detected.

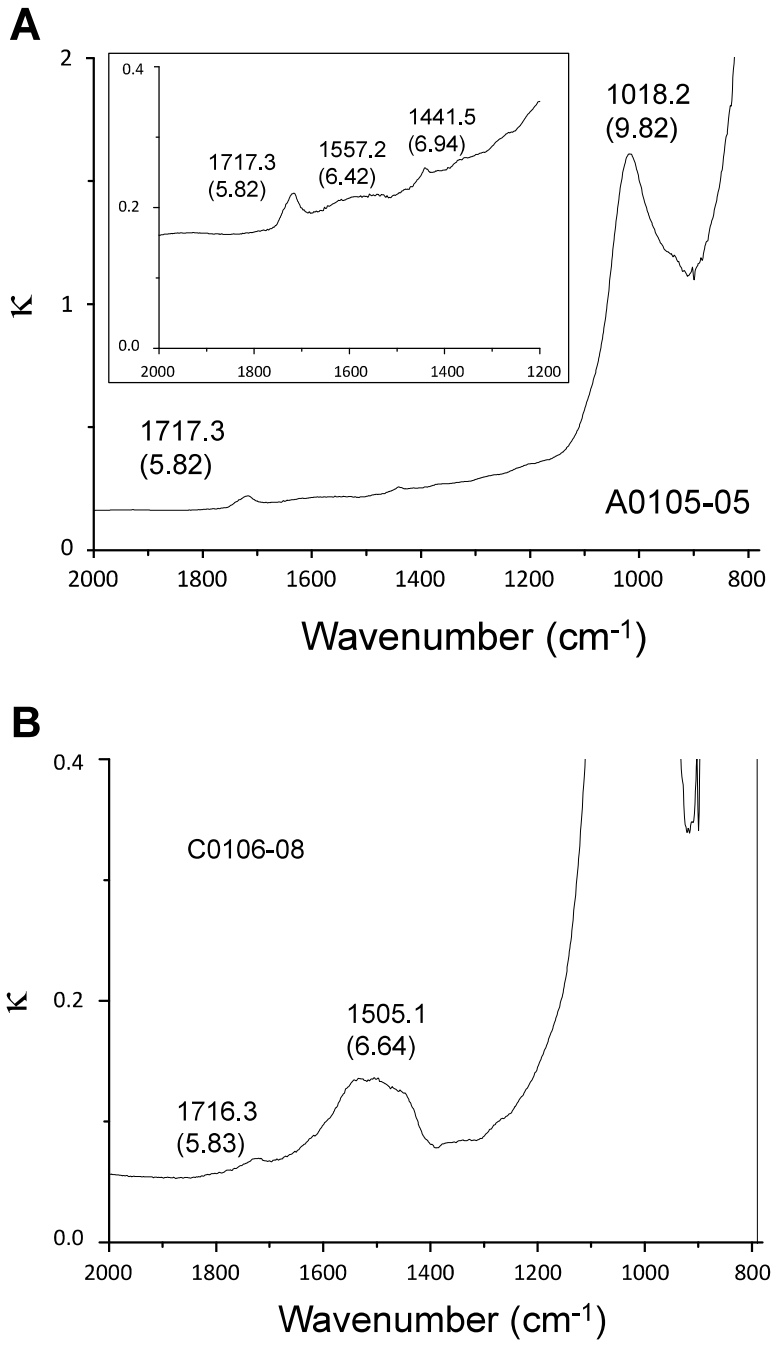

Fig. S5. Kramers-Kronig transformed FT-IR spectra of A0105-05 and C0106-08. In the region of 2000–780 cm^{-1}, the absorption at 1717.3 cm^{-1} (5.82 μm), 1557.2 cm^{-1} (6.42 μm), and 1441.5 cm^{-1} (6.94 μm) can be found in the major fraction of the spectra of allocated samples. As a typical example, Fig. S5a shows the spectrum obtained for A0105-05. Although these absorptions have not yet been assigned, the 1441.5 cm^{-1} and the 1717.3 cm^{-1} absorptions may

correspond to carbonate (*87*) and C=O stretching (*15*) respectively. The absorption due to Si-O stretching can be found at 1018.2 cm^{-1} (9.82 μm).

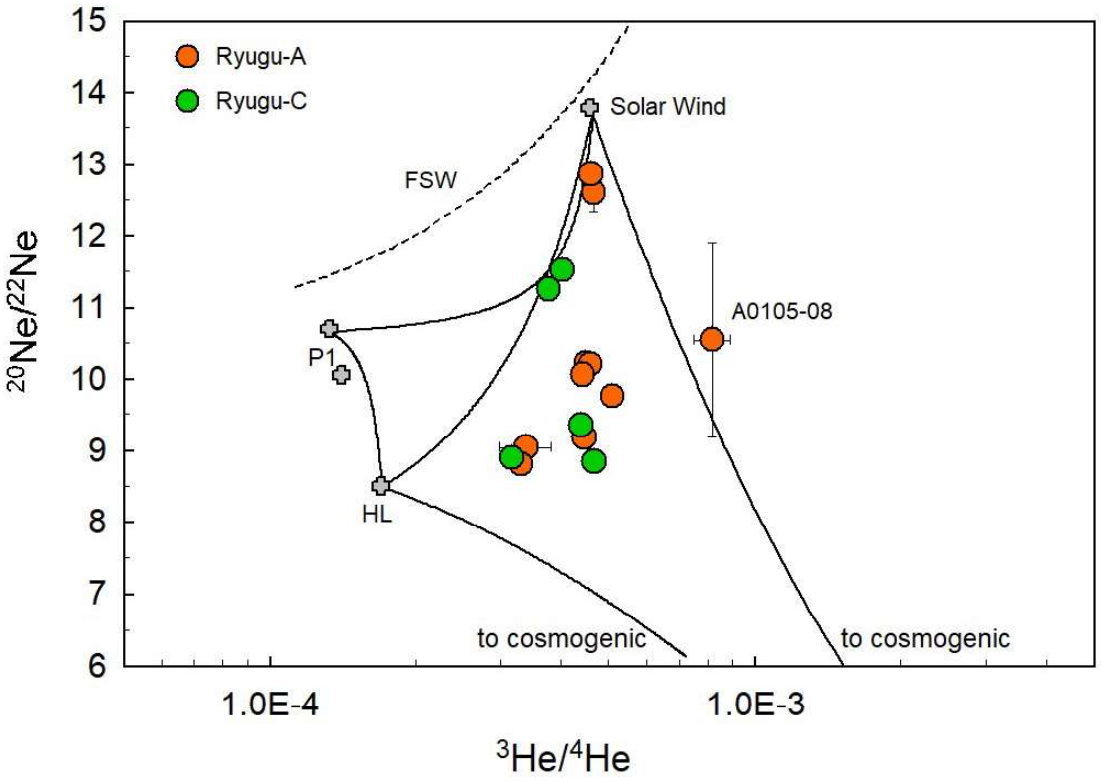

Fig. S6. Isotopic ratios of He and Ne in the Ryugu samples. The bulk isotopic ratios of He and Ne can be explained by mixing of SW, P1, HL, and cosmogenic gases. A compositional range of implantation-fractionated solar wind (FSW: *23*) calculated using TRIM simulation (*67*) is shown with a dashed line. Error bars are 1σ. Data source: *21, 22*.

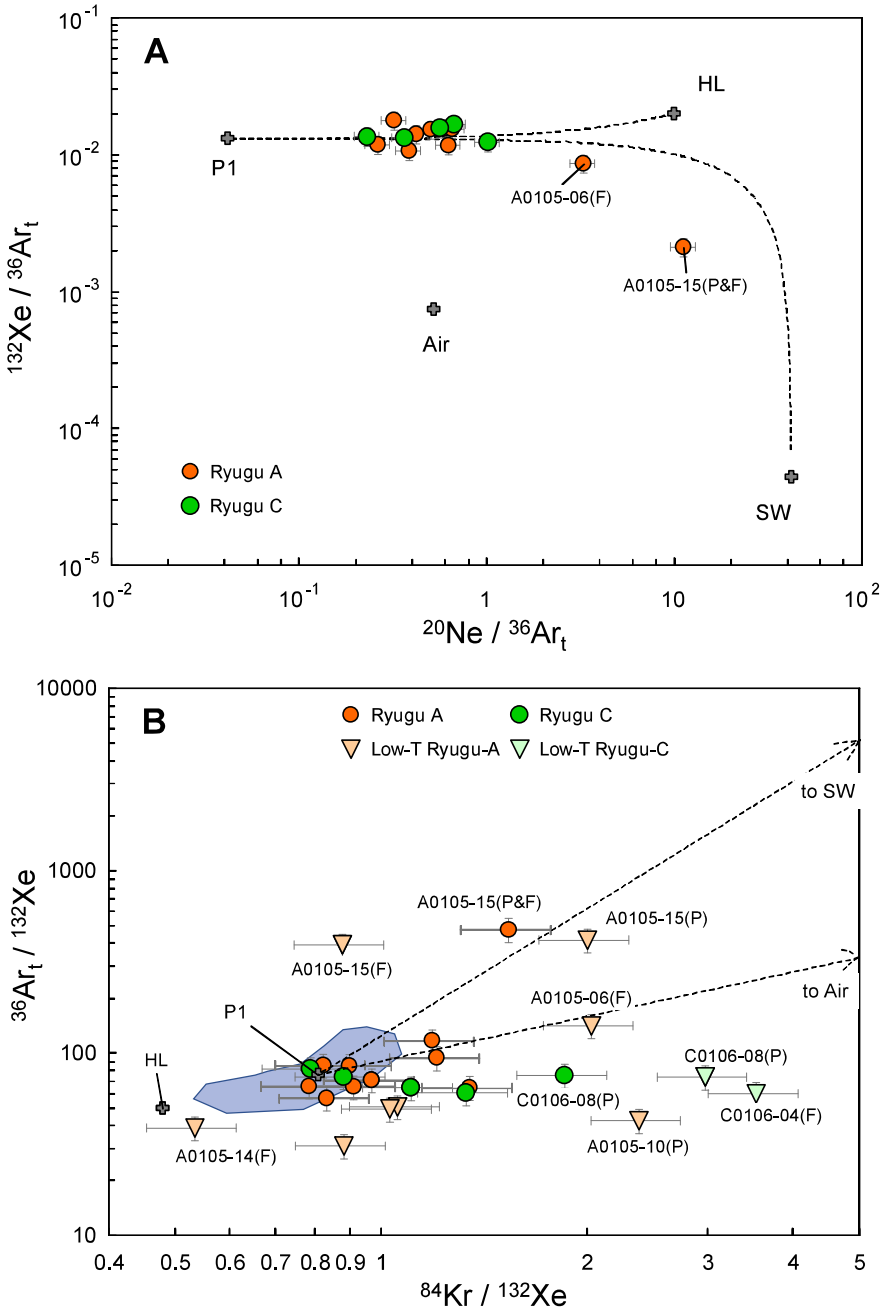

Fig. S7. Elemental ratios of noble gases. Bulk elemental ratios of noble gases can be explained by mixing of P1 and HL components. The highly solar wind (SW)-rich sample (A0105-15) is shifted towards the SW composition (A and B). There are variable contributions of elementally-fractionated terrestrial atmosphere that are evident in low temperature (low-T) fractions (B). The

blue-gray area shows a range of the P1 composition. “P” and “F” in the parentheses following each sample name denote “pelletized” and “fragmented” samples, respectively. Data sources: *20–22, 88*.

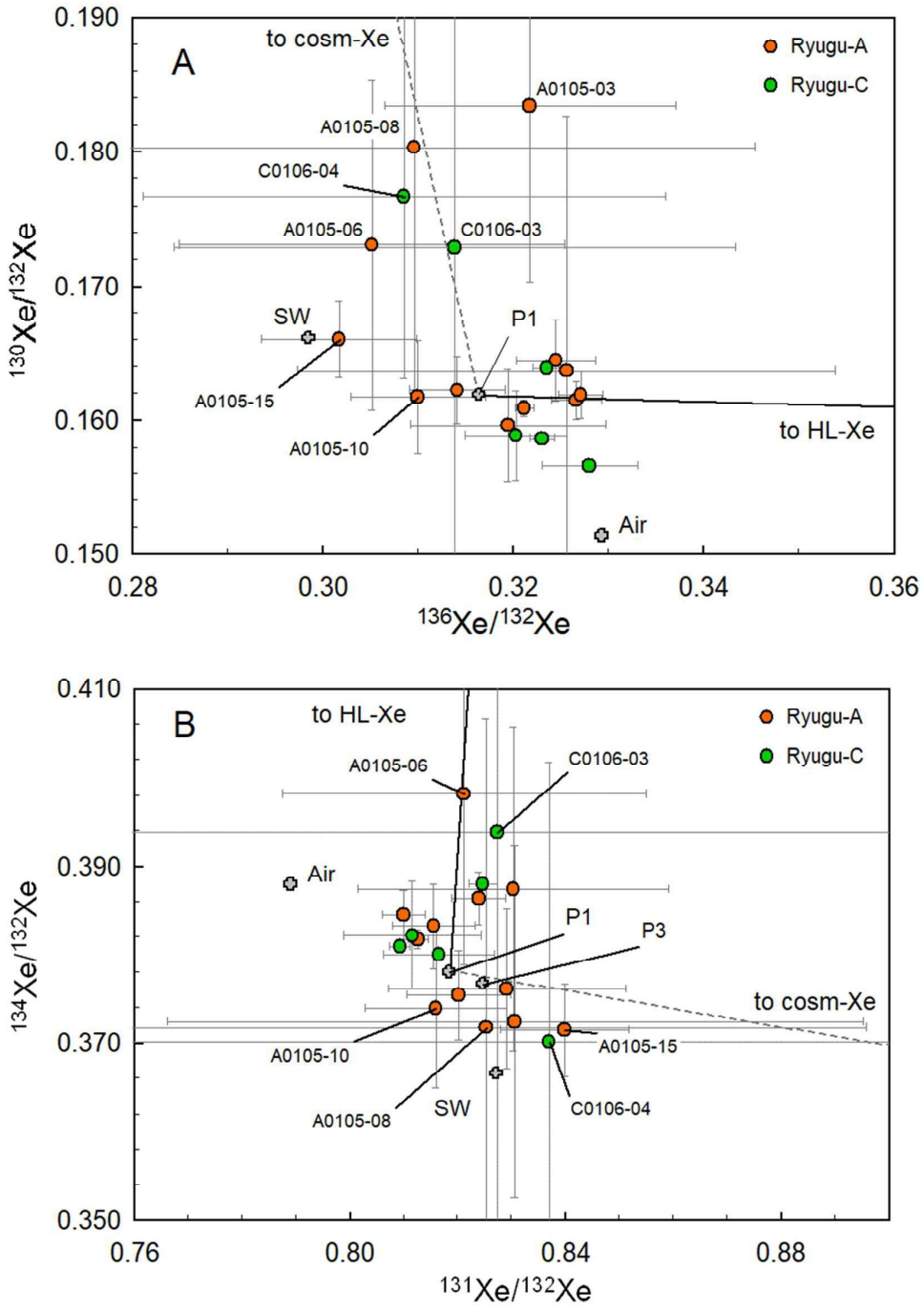

Fig. S8. Bulk Xenon isotopic ratios. The Ryugu grains contain P1-Xe as a major component, while most of the fragment samples are scattered due to their small sample weights (less than 10 μg). Data sources: *20–22, 88*. Error bars are 1σ.

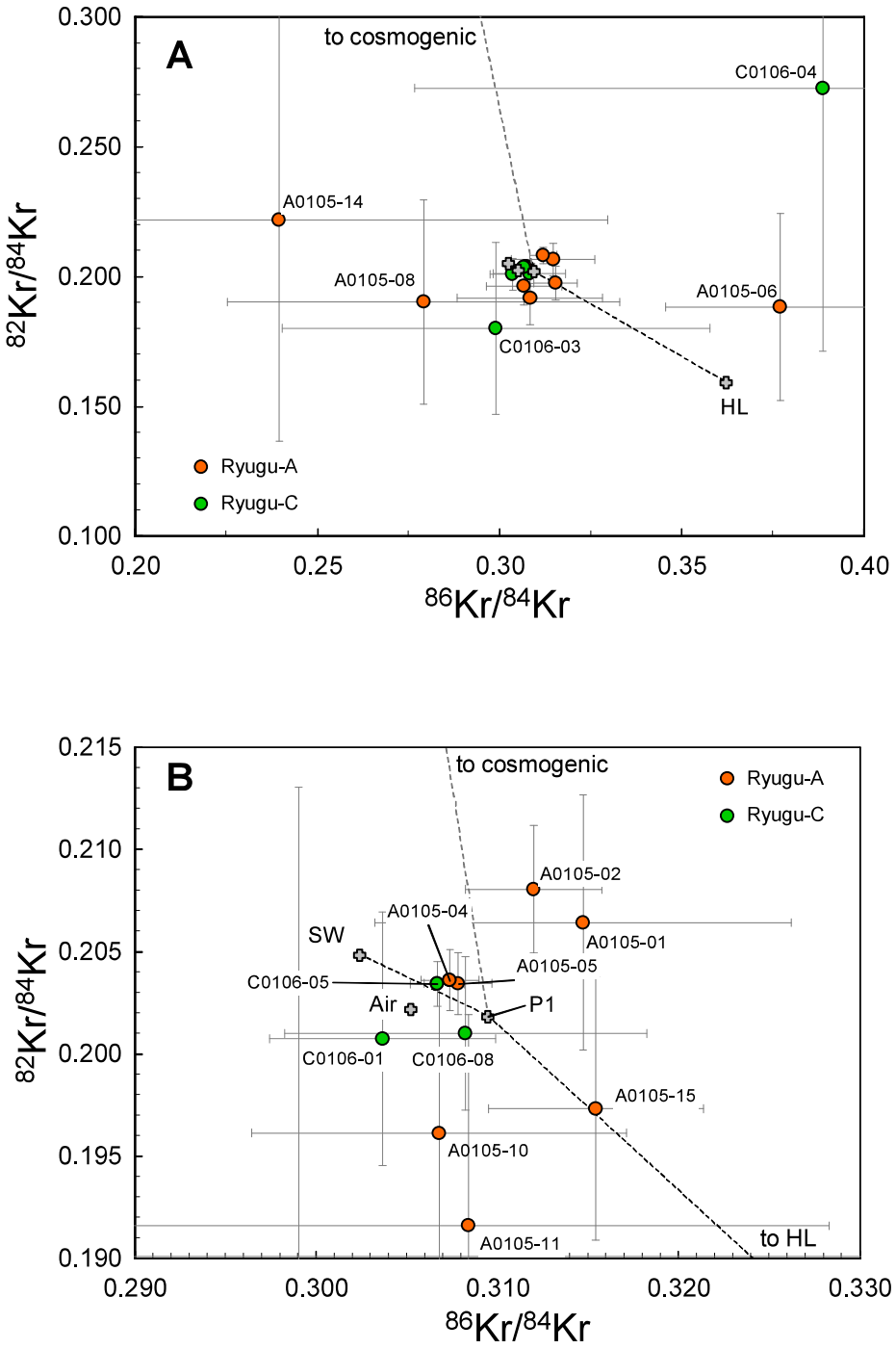

Fig. S9. Bulk Kr isotopic ratios. Most of the data plot around P1, solar wind (SW), and terrestrial atmosphere compositions, while some samples with larger uncertainties plot away

from these components (Fig. S9A). Three samples (A0105-04, -05, and C0106-05) lie on a mixing line between SW and P1 components (Fig. S9B). Data sources: *20–22, 88*.

Table S1. List of the samples allocated to the volatile sub-team.

Sample#	Weight (mg)	Laboratory	Analysis	Pellet/Fragment
A0105-01 (P)	0.1104	Kyushu U.	Noble gas	Pellet #01
A0105-06 (F)	0.0070	Kyushu U.	Noble gas	Fragment #06
A0105-08 (F)	0.0035	Kyushu U.	Noble gas	Fragment #08
A0105-10 (P)	0.0968	Kyushu U.	Noble gas	Pellet #10
A0105-10 (F)	0.0163	Kyushu U.	Noble gas	Fragment #10
A0105-11 (F)	0.0395	Kyushu U.	Noble gas	Fragment #11
A0105-14 (F)	0.0057	Kyushu U.	Noble gas	Fragment #14
A0105-15 (P)	0.1487	Kyushu U.	Noble gas	Pellet #15
A0105-15 (F)	0.0035	Kyushu U.	Noble gas	Fragment #15
C0106-03 (F)	0.0032	Kyushu U.	Noble gas	Fragment #19
C0106-04 (F)	0.0028	Kyushu U.	Noble gas	Fragment #20
C0106-08 (P)	0.1020	Kyushu U.	Noble gas	Pellet #24
A0105-02 (P)	0.1589	ETH	Noble gas	Pellet #02
C0106-01 (P)	=0.1*	ETH	Noble gas	Pellet #17
A0105-03 (P)		U. Manchester		Pellet #03
A0105-03 (F)	0.0006**	U. Manchester	Noble gas	Fragment #03
A0105-12 (P)		U. Manchester		Pellet #12
A0105-12 (F)	0.0027**	U. Manchester	Noble gas	Fragment #12

A0105-13 (P)		U. Manchester	I-Xe dating/ halogens	Pellet #13
C0106-02 (P)		U. Manchester	I-Xe dating/ halogens	Pellet #18
C0106-02 (F)	0.0115**	U. Manchester	Noble gas	Fragment #18
A0105-04 (P)	0.1729	Washington U.	Noble gas	Pellet #04
C0106-05 (P)	0.0817	Washington U.	Noble gas	Pellet #21
A0105-05 (P)	0.140	CRPG-Nancy	Noble gas /Nitrogen	Pellet #05
C0106-06 (P)	0.168	CRPG-Nancy	Noble gas /Nitrogen	Pellet #22
A0105-06 (P)		Ibaraki U.	NanoSIMS/ NAA/Ar-Ar	Pellet #06
A0105-07 (P)	0.118	Ibaraki U.	Noble gas /Nitrogen	Pellet #07
A0105-08 (P)		Ibaraki U.	NanoSIMS/ NAA/Ar-Ar	Pellet #08
A0105-11 (P)		Ibaraki U.	NanoSIMS/ NAA/Ar-Ar	Pellet #11
A0105-14 (P)		Ibaraki U.	NanoSIMS/ NAA/Ar-Ar	Pellet #14
C0106-03 (P)		Ibaraki U.	NanoSIMS/ NAA/Ar-Ar	Pellet #19
C0106-04 (P)		Ibaraki U.	NanoSIMS/ NAA/Ar-Ar	Pellet #20
C0106-07 (P)	0.119	Ibaraki U.	Noble gas /Nitrogen	Pellet #23
A0105-09 (P)		TITEC/ JAMSTEC	Volatile molecules	Pellet #09
A0105-16 (P)		TITEC/ JAMSTEC	Volatile molecules	Pellet #16
A0105-17		TITEC/ JAMSTEC	Volatile molecules	Non-processed particle

A0105-18		TITEC/ JAMSTEC	Volatile molecules	Non-processed particle
A0105-19		UC Berkeley/ KOPRI	Cosmogenic nuclides	Non-processed particle
A0105-20		UC Berkeley/ KOPRI	Cosmogenic nuclides	Non-processed particle
C0106-09		UC Berkeley/ KOPRI	Cosmogenic nuclides	Non-processed particle
C0106-10		UC Berkeley/ KOPRI	Cosmogenic nuclides	Non-processed particle
C0106-11		UC Berkeley/ KOPRI	Cosmogenic nuclides	Non-processed particle

*Nominal mass. See section SOM – Noble gas and nitrogen analyses – at ETH for details.
**Sample masses for Manchester samples were estimated from grain diameters measured photographically by assuming grains were spherical adopting a density of 1.8 g/cm^3 (*17*). "P" and "F" in the parentheses following each sample name denote "pelletized" and "fragmented" samples, respectively.

Table S2. Noble gas compositions of the Ryugu pellet samples.

Sample&Temp.	^{4}He	^{3}He/^{4}He	^{22}Ne	^{20}Ne/^{22}Ne	^{21}Ne/^{22}Ne	^{36}Ar	^{38}Ar/^{36}Ar	^{40}Ar/^{36}Ar	^{84}Kr	^{132}Xe
Kyushu Univ. data										
A0105-01(P)	**[0.1104 mg]**									
100 °C	2.13E-05	0.00036 ± 0.00023	1.91E-08	9.61 ± 0.28	0.197 ± 0.010	1.88E-07	0.1821 ± 0.0042	27.1 ± 2.6	7.53E-09	9.14E-09
200 °C	7.32E-06	0.000710 ± 0.000026	5.87E-09	10.99 ± 0.45	0.093 ± 0.014	1.14E-07	0.1800 ± 0.0044	5.73 ± 0.95	1.14E-09	6.77E-10
900 °C	5.02E-05	0.0003153 ± 0.0000074	2.22E-08	9.68 ± 0.27	0.0527 ± 0.0043	3.64E-07	0.1905 ± 0.0040	(5.60) ± (0.22)	3.69E-09	3.62E-09
1800 °C	3.97E-05	0.000289 ± 0.000013	2.42E-08	7.52 ± 0.26	0.0388 ± 0.0067	1.34E-06	0.1917 ± 0.0040	2.79 ± 0.94	1.72E-08	2.20E-08
Total	1.19E-04	0.000338 ± 0.000041	7.14E-08	9.04 ± 0.15	0.0899 ± 0.0038	2.01E-06	0.1899 ± 0.0028	5.74 ± 0.68	2.96E-08	3.54E-08
A0105-06(F)	**[0.0070 mg]**									
200 °C	7.14E-04	0.000513 ± 0.000011	5.50E-07	12.97 ± 0.35	0.0376 ± 0.0039	5.83E-07	0.1861 ± 0.0054	38.5 ± 8.9	8.42E-09	4.14E-09
1800 °C	3.80E-04	0.000376 ± 0.000012	2.18E-07	11.65 ± 0.23	0.0453 ± 0.0034	2.36E-06	0.1868 ± 0.0046	15.9 ± 8.7	2.16E-08	2.11E-08
Total	1.09E-03	0.0004657 ± 0.0000081	7.68E-07	12.60 ± 0.26	0.0397 ± 0.0030	2.94E-06	0.1867 ± 0.0038	20.4 ± 7.2	3.00E-08	2.52E-08
A0105-08(F)	**[0.0035 mg]**									
200 °C	4.75E-05	0.000779 ± 0.000094	3.72E-08	12.2 ± 2.4	0.157 ± 0.064	2.50E-07	0.1883 ± 0.0108	(97.9) ± (3.9)	2.48E-09	7.52E-09
1800 °C	8.99E-05	0.000841 ± 0.000095	4.60E-08	9.2 ± 1.5	0.093 ± 0.031	1.48E-06	0.185 ± 0.012	(77.2) ± (3.1)	1.82E-08	1.88E-08
Total	1.37E-04	0.000819 ± 0.000070	8.32E-08	10.5 ± 1.4	0.1215 ± 0.0333	1.73E-06	0.186 ± 0.010	(80.2) ± (2.7)	2.07E-08	2.63E-08
A0105-10(P)	**[0.0968 mg]**									
100 °C	4.41E-05	0.000695 ± 0.000016	3.37E-08	10.84 ± 0.16	0.141 ± 0.010	1.57E-07	0.1920 ± 0.0047	145.1 ± 6.5	1.12E-08	4.84E-09
200 °C	1.01E-05	0.000613 ± 0.000034	7.58E-09	11.58 ± 0.58	0.098 ± 0.010	6.30E-08	0.1877 ± 0.0043	59.6 ± 3.0	1.11E-09	3.20E-10
900 °C	6.34E-05	0.0003316 ± 0.0000086	3.59E-08	9.54 ± 0.13	0.0454 ± 0.0023	3.78E-07	0.1924 ± 0.0041	32.4 ± 2.1	6.28E-09	3.19E-09
1800 °C	3.17E-05	0.000304 ± 0.000011	1.56E-08	9.51 ± 0.57	0.116 ± 0.011	1.01E-06	0.1934 ± 0.0040	3.7 ± 1.4	1.65E-08	1.75E-08
Total	1.49E-04	0.0004521 ± 0.0000068	9.28E-08	10.18 ± 0.13	0.0961 ± 0.0042	1.61E-06	0.1928 ± 0.0028	26.4 ± 1.2	3.51E-08	2.59E-08
A0105-10(F)	**[0.0163 mg]**									
200 °C	6.82E-05	0.000616 ± 0.000027	4.47E-08	11.32 ± 0.42	0.1011 ± 0.0083	1.78E-07	0.1737 ± 0.0053	42 ± 12	3.76E-09	3.55E-09
600 °C		0.00037 ± 0.00016				2.16E-09				
1800 °C	8.08E-05	0.000277 ± 0.000014	4.20E-08	9.62 ± 0.62	0.0248 ± 0.0076	1.15E-06	0.1885 ± 0.0053	(28.6) ± (1.1)	1.42E-08	1.06E-08
Total	1.50E-04	0.000432 ± 0.000015	8.67E-08	10.49 ± 0.37	0.0642 ± 0.0056	1.33E-06	0.1862 ± 0.0046	30.3 ± 1.9	1.80E-08	1.42E-08
A0105-10 weighted average	1.49E-04	0.0004492 ± 0.0000062	9.19E-08	10.22 ± 0.12	0.0915 ± 0.0037	1.57E-06	0.1919 ± 0.0025	27.0 ± 1.1	3.26E-08	2.42E-08
A0105-11(F)	**[0.0395 mg]**									
200 °C	6.93E-05	0.000650 ± 0.000016	5.56E-08	11.29 ± 0.20	0.1517 ± 0.0071	2.85E-07	0.1906 ± 0.0043	30.64 ± 3.56	5.96E-09	5.78E-09
1800 °C	1.01E-04	0.000328 ± 0.000010	5.16E-08	9.03 ± 0.13	0.0615 ± 0.0036	1.38E-06	0.190 ± 0.004	3.5 ± 2.7	1.73E-08	1.97E-08
Total	1.70E-04	0.0004592 ± 0.0000088	1.07E-07	10.20 ± 0.12	0.1083 ± 0.0041	1.67E-06	0.1902 ± 0.0035	8.1 ± 2.3	2.33E-08	2.55E-08

(Table S2 continued)

Sample&Temp.	^{4}He	^{3}He/^{4}He	^{22}Ne	^{20}Ne/^{22}Ne	^{21}Ne/^{22}Ne	^{36}Ar	^{38}Ar/^{36}Ar	^{40}Ar/^{36}Ar	^{84}Kr	^{132}Xe
Kyushu Univ. data										
A0105-14(F)	**[0.0057 mg]**									
200 °C	2.52E-05	0.000824 ± 0.000072	2.44E-08	7.9 ± 1.2	0.204 ± 0.044	2.24E-07	0.1968 ± 0.0100	(89.6) ± (3.7)	3.07E-09	5.74E-09
1800 °C	6.35E-05	0.000296 ± 0.000029	2.82E-08	10.3 ± 2.1	0.076 ± 0.027	1.03E-06	0.191 ± 0.006	(69.9) ± (2.8)	1.30E-08	7.55E-09
Total	8.87E-05	0.000446 ± 0.000029	5.26E-08	9.2 ± 1.3	0.135 ± 0.025	1.25E-06	0.1921 ± 0.0050	(73.4) ± (2.4)	1.61E-08	1.33E-08
A0105-15(P)	**[0.1487 mg]**									
100 °C	4.03E-03	0.000508 ± 0.000010	4.06E-06	13.031 ± .064	0.03142 ± 0.0007	1.84E-06	0.1861 ± 0.0039	14.8 ± .6	1.16E-08	6.52E-09
200 °C	8.51E-04	0.000384 ± 0.000010	2.81E-06	12.96 ± 0.12	0.0314 ± 0.0014	1.22E-06	0.1898 ± 0.0040	7.75 ± 0.32	3.14E-09	8.32E-10
900 °C	7.75E-04	0.000318 ± 0.000016	5.36E-06	12.771 ± 0.078	0.03174 ± 0.00073	8.90E-06	0.1890 ± 0.0040	0.91 ± 0.06	1.24E-08	3.63E-09
1800 °C	5.76E-05	0.0002883 ± 0.0000077	1.76E-07	11.10 ± 0.16	0.03578 ± 0.00093	2.25E-06	0.1909 ± 0.0039	1.54 ± 0.42	1.91E-08	1.89E-08
Total	5.71E-03	0.000461 ± 0.000008	1.24E-05	12.87 ± 0.05	0.0316 ± 0.0005	1.42E-05	0.1890 ± 0.0026	3.39 ± 0.12	4.62E-08	2.99E-08
A0105-15(F)	**[0.0035 mg]**									
200 °C	3.18E-03	0.000465 ± 0.000010	4.62E-06	12.56 ± 0.06	0.031 ± 0.001	2.44E-06	0.1843 ± 0.0066	(14.82) ± (0.73)	5.50E-09	6.26E-09
1800 °C	6.56E-04	0.000298 ± 0.000006	5.41E-06	12.46 ± 0.12	0.032 ± 0.002	8.89E-06	0.189 ± 0.004	(17.60) ± (0.70)	2.08E-08	1.94E-08
Total	3.84E-03	0.0004363 ± 0.0000080	1.00E-05	12.507 ± 0.069	0.0312 ± 0.0011	1.13E-05	0.1883 ± 0.0036	(17.00) ± (0.57)	2.63E-08	2.57E-08
A0105-15 weighted average	5.67E-03	0.0004607 ± 0.0000077	1.24E-05	12.87 ± 0.05	0.0316 ± 0.0005	1.41E-05	0.1890 ± 0.0026	3.7 ± 0.1	4.58E-08	2.98E-08
C0106-03(F)	**[0.0032 mg]**									
200 °C	1.03E-04	0.000603 ± 0.000038	6.47E-08	12.2 ± 1.0	0.081 ± 0.019	2.23E-07	0.2022 ± 0.0154	116.98 ± 35.58		3.20E-09
1800 °C	1.47E-04	0.000262 ± 0.000017	1.00E-07	11.1 ± 1.2	0.051 ± 0.018	1.65E-06	0.192 ± 0.006	(87.7) ± (3.5)	1.80E-08	1.96E-08
Total	2.50E-04	0.000402 ± 0.000018	1.65E-07	11.52 ± 0.83	0.0630 ± 0.0131	1.87E-06	0.1934 ± 0.0054	91.2 ± 5.2	1.80E-08	2.28E-08
C0106-04(F)	**[0.0028 mg]**									
200 °C	5.67E-05	0.000554 ± 0.000079	4.94E-08	11.6 ± 1.6	0.081 ± 0.039	2.72E-07	0.2057 ± 0.0135	(120.6) ± (5.4)	1.59E-08	4.49E-09
1800 °C	7.51E-05	0.000243 ± 0.000022	3.11E-08	10.6 ± 3.3	0.094 ± 0.037	1.08E-06	0.190 ± 0.008	(118.4) ± (4.7)	1.38E-08	1.78E-08
Total	1.32E-04	0.000377 ± 0.000036	8.05E-08	11.2 ± 1.6	0.086 ± 0.028	1.35E-06	0.1935 ± 0.0069	(118.8) ± (3.9)	2.97E-08	2.23E-08
C0106-8(P)	**[0.1020 mg]**									
200 °C	3.85E-05	0.000755 ± 0.000016	3.25E-08	9.29 ± 0.24	0.1723 ± 0.0058	3.56E-07	0.1885 ± 0.0042	162.5 ± 7.1	1.44E-08	4.83E-09
1800 °C	8.49E-05	0.000337 ± 0.000008	4.65E-08	8.53 ± 0.13	0.0677 ± 0.0040	1.55E-06	0.190 ± 0.004	18.7 ± 1.3	3.25E-08	2.04E-08
Total	1.23E-04	0.000468 ± 0.000008	7.90E-08	8.84 ± 0.12	0.1107 ± 0.0034	1.91E-06	0.1897 ± 0.0033	45.6 ± 1.7	4.69E-08	2.52E-08

(Table S2 continued)

Sample	^{4}He	^{3}He/^{4}He	^{22}Ne	^{20}Ne/^{22}Ne	^{21}Ne/^{22}Ne	^{36}Ar	^{38}Ar/^{36}Ar	^{40}Ar/^{36}Ar	^{84}Kr	^{132}Xe
CRPG-Nancy data										
A0105-05	**[0.140mg]**									
Total	1.70E-04	0.000442 ± 0.000012	9.09E-08	10.06 ± 0.15	0.0730 ± 0.0013	1.46E-06	0.18705 ± 0.00045	3.544 ± 0.070	1.40E-08	1.70E-08
C0106-06	**[0.168mg]**									
Total			4.99E-08	9.087 ± 0.099	0.0953 ± 0.0033	1.14E-06	0.17854 ± 0.00074	13.72 ± 0.59		

Sample&Temp.	^{4}He	^{3}He/^{4}He	^{22}Ne	^{20}Ne/^{22}Ne	^{21}Ne/^{22}Ne	^{36}Ar	^{38}Ar/^{36}Ar	^{40}Ar/^{36}Ar	^{84}Kr	^{132}Xe
ETH data										
A0105-02	**[0.1589 mg]**									
Step-1	1.05E-04	0.000330 ± 0.000010	6.07E-08	8.78 ± 0.17	0.1020 ± 0.0073	1.74E-06	0.18868 ± 0.00070	3.20 ± 0.30	1.83E-08	1.92E-08
Step-2	n.d.		1.48E-09	11.1 ± 2.3	0.0634 ± 0.0474	3.83E-07	0.1883 ± 0.0010	11.80 ± 0.30	3.78E-09	5.62E-09
Step-3	n.d.		1.83E-09	8.0 ± 1.4	0.0733 ± 0.0499	6.70E-09	0.226 ± 0.046	173 ± 33	4.40E-10	2.20E-10
Total	1.05E-04	0.000330 ± 0.000010	6.40E-08	8.81 ± 0.17	0.1003 ± 0.0072	2.13E-06	0.18873 ± 0.00062	5.28 ± 0.27	2.25E-08	2.50E-08
C0106-01	**[0.1 mg]**									
Step-1	4.37E-05	0.000316 ± 0.000042	2.66E-08	8.9 ± 2.0	0.0930 ± 0.0020	1.08E-06	0.1890 ± 0.0015	14.1 ± 1.2	1.29E-08	1.47E-08
Step-2	n.d.		2.43E-09	7.3 ± 2.7		1.15E-08	0.216 ± 0.018	127.5 ± 9.5	1.44E-10	1.60E-10
Total	4.37E-05	0.000316 ± 0.000042	2.90E-08	8.7 ± 1.8	0.0852 ± 0.0018	1.10E-06	0.1893 ± 0.0015	15.3 ± 1.2	1.31E-08	1.48E-08
Murchison	**[0.0632 mg]**									
Step-1	6.35E-05	0.000504 ± 0.000039	5.08E-08	5.6 ± 1.3	0.279 ± 0.047	1.11E-06	0.1880 ± 0.0020	3.90 ± 1.80	1.12E-08	1.35E-08
Step-2	n.d.		1.79E-08	8.71 ± 0.80	0.0275 ± 0.0057	4.19E-08	0.1751 ± 0.0064	12.80 ± 1.10	4.27E-10	4.70E-10
Total	6.35E-05	0.000504 ± 0.000039	6.86E-08	6.43 ± 0.96	0.214 ± 0.035	1.15E-06	0.1875 ± 0.0019	4.2 ± 1.7	1.16E-08	1.40E-08

Sample	^{4}He	^{3}He/^{4}He	^{22}Ne	^{20}Ne/^{22}Ne	^{21}Ne/^{22}Ne	^{36}Ar	^{38}Ar/^{36}Ar	^{40}Ar/^{36}Ar	^{84}Kr	^{132}Xe
Washington U. data										
A0105-04	**[0.1729 mg]**									
Total	1.16E-04	0.00051 ± 0.00010	7.12E-08	9.76 ± 0.13	0.097 0.002	1.64E-06	0.1869 ± 0.0005	31.9	2.24E-08	2.31E-08
C0106-05	**[0.0817 mg]**									
Total	1.97E-04	0.00044 ± 0.0002	1.23E-07	9.35 ± 0.15	0.062 ± 0.002	2.03E-06	0.1892 ± 0.0007	51.3	3.49E-08	3.15E-08

(Table S2 continued)

Sample&Temp.	^{84}Kr	^{78}Kr/^{84}Kr	^{80}Kr/^{84}Kr	^{82}Kr/^{84}Kr	^{83}Kr/^{84}Kr	^{86}Kr/^{84}Kr
Kyushu Univ. data						
A0105-01(P)	**[0.1104 mg]**					
100 °C	7.53E-09	0.0066 ± 0.0019	0.0412 ± 0.0055	0.199 ± 0.014	0.202 ± 0.015	0.306 ± 0.020
200 °C	1.14E-09	0.016 ± 0.013	0.036 ± 0.017	0.194 ± 0.035	0.205 ± 0.042	0.338 ± 0.073
900 °C	3.69E-09	0.0067 ± 0.0020	0.0418 ± 0.0076	0.211 ± 0.017	0.201 ± 0.014	0.322 ± 0.024
1800 °C	1.72E-08	0.0075 ± 0.0021	0.0408 ± 0.0060	0.2097 ± 0.0075	0.2034 ± 0.0084	0.315 ± 0.016
Total	2.96E-08	0.0075 ± 0.0015	0.0408 ± 0.0039	0.2064 ± 0.0062	0.2028 ± 0.0067	0.315 ± 0.011
A0105-06(F)	**[0.0070 mg]**					
200 °C	8.42E-09	0.042 ± 0.028	0.048 ± 0.034	0.20 ± 0.10	0.182 ± 0.088	0.532 ± 0.069
1800 °C	2.16E-08	0.0161 ± 0.0079	0.0379 ± 0.0172	0.182 ± 0.030	0.220 ± 0.045	0.317 ± 0.035
Total	3.00E-08	0.0234 ± 0.0097	0.041 ± 0.016	0.188 ± 0.036	0.209 ± 0.041	0.377 ± 0.032
A0105-08(F)	**[0.0035 mg]**					
200 °C	2.48E-09	(0.039) ± (0.025)	(0.044) ± (0.024)	(0.164) ± (0.081)	(0.113) ± (0.056)	(0.261) ± (0.064)
1800 °C	1.82E-08	0.031 ± 0.030	0.034 ± 0.029	0.194 ± 0.043	0.181 ± 0.051	0.282 ± 0.061
Total	2.07E-08	0.032 ± 0.026	0.035 ± 0.025	0.190 ± 0.039	0.173 ± 0.046	0.279 ± 0.054
A0105-10(P)	**[0.0968 mg]**					
100 °C	1.12E-08	0.0082 ± 0.0019	0.0345 ± 0.0016	0.203 ± 0.011	0.2023 ± 0.0093	0.312 ± 0.018
200 °C	1.11E-09	0.0192 ± 0.0060	0.044 ± 0.023	0.202 ± 0.043	0.212 ± 0.048	0.283 ± 0.041
900 °C	6.28E-09	0.026 ± 0.014	0.038 ± 0.013	0.197 ± 0.023	0.204 ± 0.026	0.291 ± 0.036
1800 °C	1.65E-08	0.0038 ± 0.0012	0.0328 ± 0.0057	0.1952 ± 0.0096	0.201 ± 0.013	0.313 ± 0.012
Total	3.51E-08	0.0096 ± 0.0027	0.0345 ± 0.0037	0.1984 ± 0.0072	0.2022 ± 0.0083	0.308 ± 0.010
A0105-10(F)	**[0.0163 mg]**					
200 °C	3.76E-09	0.017 ± 0.013	0.025 ± 0.015	0.155 ± 0.032	0.170 ± 0.046	0.313 ± 0.089
600 °C	0.00E+00					
1800 °C	1.42E-08	0.0035 ± 0.0052	0.0213 ± 0.0086	0.190 ± 0.031	0.196 ± 0.026	0.299 ± 0.041
Total	1.80E-08	0.0062 ± 0.0049	0.0220 ± 0.0075	0.183 ± 0.025	0.191 ± 0.023	0.302 ± 0.038
A0105-10 weighted average	3.26E-08	0.0091 ± 0.0024	0.0327 ± 0.0033	0.1961 ± 0.0072	0.2005 ± 0.0079	0.3068 ± 0.0104
A0105-11(F)	**[0.0395 mg]**					
200 °C	5.96E-09	0.008 ± 0.008	0.046 ± 0.012	0.174 ± 0.028	0.204 ± 0.024	0.310 ± 0.040
1800 °C	1.73E-08	0.007 ± 0.004	0.036 ± 0.008	0.197 ± 0.010	0.197 ± 0.016	0.308 ± 0.023
Total	2.33E-08	0.0075 ± 0.0039	0.0383 ± 0.0068	0.192 ± 0.010	0.199 ± 0.013	0.308 ± 0.020

(Table S2 continued)

Sample&Temp.	^{84}Kr	^{78}Kr/^{84}Kr	^{80}Kr/^{84}Kr	^{82}Kr/^{84}Kr	^{83}Kr/^{84}Kr	^{86}Kr/^{84}Kr
Kyushu Univ. data						
A0105-14(F)	**[0.0057 mg]**					
200 °C	3.07E-09	0.078 ± 0.033	(0.041) ± (0.020)	0.28 ± 0.18	0.20 ± 0.13	0.39 ± 0.25
1800 °C	1.30E-08	0.031 ± 0.026	0.041 ± 0.021	0.207 ± 0.096	0.214 ± 0.090	0.204 ± 0.094
Total	1.61E-08	0.040 ± 0.022	0.041 ± 0.018	0.222 ± 0.085	0.212 ± 0.077	0.240 ± 0.090
A0105-15(P)	**[0.1487 mg]**					
100 °C	1.16E-08	0.0064 ± 0.0017	0.0369 ± 0.0028	0.195 ± 0.014	0.193 ± 0.011	0.3114 ± 0.0095
200 °C	3.14E-09	0.0143 ± 0.0058	0.0394 ± 0.0066	0.225 ± 0.026	0.187 ± 0.026	0.365 ± 0.042
900 °C	1.24E-08	0.0060 ± 0.0015	0.0340 ± 0.0044	0.189 ± 0.011	0.190 ± 0.010	0.3116 ± 0.0087
1800 °C	1.91E-08	0.0065 ± 0.0012	0.0383 ± 0.0016	0.1996 ± 0.0099	0.1992 ± 0.0064	0.3123 ± 0.0090
Total	4.62E-08	0.00686 ± 0.00086	0.0368 ± 0.0016	0.1975 ± 0.0064	0.1945 ± 0.0050	0.3155 ± 0.0057
A0105-15(F)	**[0.0035 mg]**					
200 °C	5.50E-09		(0.041) ± (0.021)	0.176 ± 0.063	0.187 ± 0.086	0.299 ± 0.168
1800 °C	2.08E-08	0.016 ± 0.011	0.050 ± 0.023	0.191 ± 0.077	0.217 ± 0.054	0.319 ± 0.099
Total	2.63E-08	0.016 ± 0.011	0.048 ± 0.018	0.187 ± 0.063	0.211 ± 0.046	0.315 ± 0.086
A0105-15 weighted average	4.58E-08	0.00708 ± 0.00088	0.03711 ± 0.00161	0.19732 ± 0.00644	0.19489 ± 0.00495	0.31545 ± 0.00594
C0106-03(F)	**[0.0032 mg]**					
200 °C						
1800 °C	1.80E-08	0.025 ± 0.022	0.043 ± 0.027	0.180 ± 0.033	0.209 ± 0.048	0.299 ± 0.059
Total	1.80E-08	0.025 ± 0.022	0.043 ± 0.027	0.180 ± 0.033	0.209 ± 0.048	0.299 ± 0.059
C0106-04(F)	**[0.0028 mg]**					
200 °C	1.59E-08	0.043 ± 0.041	0.078 ± 0.043	0.26 ± 0.15	0.199 ± 0.059	0.298 ± 0.087
1800 °C	1.38E-08	0.056 ± 0.039	0.065 ± 0.042	0.28 ± 0.13	0.17 ± 0.12	0.49 ± 0.22
Total	2.97E-08	0.049 ± 0.029	0.072 ± 0.030	0.27 ± 0.10	0.185 ± 0.063	0.39 ± 0.11
C0106-8(P)	**[0.1020 mg]**					
200 °C	1.44E-08	0.0078 ± 0.0014	0.0399 ± 0.0053	0.2020 ± 0.0080	0.199 ± 0.013	0.303 ± 0.022
1800 °C	3.25E-08	0.0064 ± 0.0013	0.0386 ± 0.0044	0.2005 ± 0.0041	0.1966 ± 0.0073	0.311 ± 0.011
Total	4.69E-08	0.0069 ± 0.0010	0.0390 ± 0.0035	0.2010 ± 0.0037	0.1972 ± 0.0066	0.308 ± 0.010

(Table S2 continued)

Sample	^{84}Kr	^{78}Kr/^{84}Kr	^{80}Kr/^{84}Kr	^{82}Kr/^{84}Kr	^{83}Kr/^{84}Kr	^{86}Kr/^{84}Kr
CRPG-Nancy data						
A0105-05	**[0.140 mg]**					
Total	1.40E-08	0.00629 ± 0.00015	0.04013 ± 0.00042	0.2034 ± 0.0015	0.2035 ± 0.0011	0.3078 ± 0.0019

Sample&Temp.	^{84}Kr	^{78}Kr/^{84}Kr	^{80}Kr/^{84}Kr	^{82}Kr/^{84}Kr	^{83}Kr/^{84}Kr	^{86}Kr/^{84}Kr
ETH data						
A0105-02	**[0.1589 mg]**					
step-1	1.83E-08	0.00274 ± 0.00057	0.0384 ± 0.0011	0.2082 ± 0.0033	0.1976 ± 0.0042	0.3120 ± 0.0038
step-2	3.78E-09		0.0405 ± 0.0022	0.2082 ± 0.0085	0.193 ± 0.008	0.321 ± 0.011
step-3	4.40E-10		0.043 ± 0.012	0.199 ± 0.037	0.2454 ± 0.0342	0.240 ± 0.055
Total	2.25E-08	0.00274 ± 0.00057	0.0388 ± 0.0010	0.2080 ± 0.0031	0.1978 ± 0.0038	0.3120 ± 0.0038
C0106-01	**[0.1 mg]**					
step-1	1.29E-08	0.00579 ± 0.00074	0.0357 ± 0.0020	0.1972 ± 0.0053	0.1986 ± 0.0059	0.3025 ± 0.0057
step-2	1.44E-10			0.52 ± 0.29		0.41 0.25
Total	1.31E-08	0.00579 ± 0.00074	0.0357 ± 0.0020	0.2007 ± 0.0062	0.1986 ± 0.0059	0.3037 ± 0.0063
Murchison	**[0.0632 mg]**					
step-1	1.12E-08	0.0037 ± 0.0015	0.0394 ± 0.0027	0.2092 ± 0.0078	0.1945 ± 0.0092	0.3239 ± 0.0075
step-2	4.27E-10		0.039 ± 0.030	0.238 ± 0.085	0.150 ± 0.094	0.300 ± 0.095
Total	1.16E-08	0.0037 ± 0.0015	0.0394 ± 0.0027	0.2092 ± 0.0078	0.1945 ± 0.0092	0.3239 ± 0.0075

Sample	^{84}Kr	^{78}Kr/^{84}Kr	^{80}Kr/^{84}Kr	^{82}Kr/^{84}Kr	^{83}Kr/^{84}Kr	^{86}Kr/^{84}Kr
Washington U. data						
A0105-04	**[0.1729 mg]**					
Total	2.24E-08	< 0.0085	0.0400 ± 0.0005	0.2036 ± 0.0015	0.2007 ± 0.0011	0.3074 ± 0.0016
C0106-05	**[0.0817 mg]**					
Total	3.49E-08	< 0.0074	0.0399 ± 0.0005	0.2034 ± 0.0011	0.20083 ± 0.00083	0.3067 ± 0.0015

(Table S2 continued)

Sample&Temp.	^{132}Xe	^{124}Xe/^{132}Xe	^{126}Xe/^{132}Xe	^{128}Xe/^{132}Xe	^{129}Xe/^{132}Xe	^{130}Xe/^{132}Xe	^{131}Xe/^{132}Xe	^{134}Xe/^{132}Xe	^{136}Xe/^{132}Xe
Kyushu Univ. data									
A0105-01(P)	**[0.1104 mg]**								
100 °C	9.14E-09	0.0040 ± 0.0013	0.0039 ± 0.0013	0.0761 ± 0.0077	1.036 ± 0.022	0.1565 ± 0.0051	0.811 ± 0.021	0.379 ± 0.014	0.3211 ± 0.0093
200 °C	6.77E-10	0.0049 ± 0.0038	0.0068 ± 0.0078	0.0880 ± 0.0227	1.0340 ± 0.0837	0.1641 ± 0.0190	0.8084 ± 0.0663	0.3867 ± 0.0282	0.3215 ± 0.0206
900 °C	3.62E-09	0.0031 ± 0.0012	0.0042 ± 0.0013	0.07711 ± 0.00651	1.072 ± 0.038	0.1642 ± 0.0116	0.822 ± 0.031	0.3688 ± 0.0169	0.3065 ± 0.0119
1800 °C	2.20E-08	0.00272 ± 0.00094	0.00390 ± 0.00095	0.0808 ± 0.0034	1.050 ± 0.012	0.1642 ± 0.0028	0.824 ± 0.012	0.3744 ± 0.0051	0.3123 ± 0.0068
Total	3.54E-08	0.00313 ± 0.00069	0.00399 ± 0.00070	0.0793 ± 0.0030	1.0485 ± 0.0102	0.1622 ± 0.0025	0.8203 ± 0.0096	0.3754 ± 0.0051	0.3142 ± 0.0050
A0105-06(F)	**[0.0070 mg]**								
200 °C	4.14E-09	0.0142 ± 0.0087	0.022 ± 0.022	0.077 ± 0.043	1.08 ± 0.14	0.182 ± 0.047	0.819 ± 0.078	0.380 ± 0.059	0.309 ± 0.064
1800 °C	2.11E-08	0.0093 ± 0.0059	0.0063 ± 0.0037	0.091 ± 0.019	1.055 ± 0.064	0.171 ± 0.012	0.822 ± 0.037	0.402 ± 0.020	0.304 ± 0.021
Total	2.52E-08	0.0101 ± 0.0052	0.0088 ± 0.0047	0.0884 ± 0.0176	1.059 ± 0.058	0.1730 ± 0.0124	0.821 ± 0.034	0.398 ± 0.019	0.305 ± 0.020
A0105-08(F)	**[0.0035 mg]**								
200 °C	7.52E-09	0.0142 ± 0.0088	0.022 ± 0.022	0.077 ± 0.044	1.08 ± 0.14	0.182 ± 0.047	0.819 ± 0.078	0.380 ± 0.060	0.309 ± 0.064
1800 °C	1.88E-08	0.0123 ± 0.0080	0.0050 ± 0.0075	0.080 ± 0.023	1.112 ± 0.068	0.180 ± 0.017	0.828 ± 0.094	0.369 ± 0.042	0.310 ± 0.043
Total	2.63E-08	0.0128 ± 0.0062	0.0098 ± 0.0082	0.0788 ± 0.0208	1.102 ± 0.063	0.1803 ± 0.0183	0.825 ± 0.071	0.372 ± 0.035	0.310 ± 0.036
A0105-10(P)	**[0.0968 mg]**								
100 °C	4.84E-09	0.0016 ± 0.0013	0.0023 ± 0.0018	0.0683 ± 0.0090	0.955 ± 0.045	0.1499 ± 0.0075	0.792 ± 0.020	0.379 ± 0.033	0.322 ± 0.024
200 °C	3.20E-10	0.022 ± 0.020	0.0057 ± 0.0074	0.074 ± 0.033	0.827 ± 0.207	0.158 ± 0.014	0.813 ± 0.031	0.369 ± 0.050	0.306 ± 0.038
900 °C	3.19E-09	0.0131 ± 0.0037	0.0084 ± 0.0035	0.088 ± 0.019	1.079 ± 0.084	0.166 ± 0.026	0.825 ± 0.061	0.360 ± 0.043	0.299 ± 0.034
1800 °C	1.75E-08	0.00189 ± 0.00082	0.0038 ± 0.0012	0.0815 ± 0.0038	1.072 ± 0.017	0.1648 ± 0.0045	0.820 ± 0.017	0.3753 ± 0.0091	0.3113 ± 0.0074
Total	2.59E-08	0.00347 ± 0.00080	0.00411 ± 0.00098	0.0797 ± 0.0039	1.048 ± 0.018	0.1621 ± 0.0046	0.815 ± 0.014	0.374 ± 0.010	0.3116 ± 0.0080
A0105-10(F)	**[0.0163 mg]**								
200 °C	3.55E-09	0.0102 ± 0.0086	0.0073 ± 0.0042	0.0715 ± 0.0080	0.990 ± 0.081	0.151 ± 0.040	0.78 ± 0.10	0.383 ± 0.021	0.317 ± 0.018
600 °C	0.00E+00								
1800 °C	1.06E-08	0.0022 ± 0.0018	0.0027 ± 0.0013	0.0781 ± 0.0094	1.032 ± 0.057	0.1625 ± 0.0030	0.834 ± 0.033	0.369 ± 0.016	0.295 ± 0.013
Total	1.42E-08	0.0042 ± 0.0026	0.0039 ± 0.0014	0.0765 ± 0.0073	1.022 ± 0.047	0.160 ± 0.010	0.821 ± 0.036	0.373 ± 0.013	0.301 ± 0.011
A0105-10 weighted average	2.42E-08	0.00357 ± 0.00078	0.00408 ± 0.00086	0.0793 ± 0.0035	1.044 ± 0.017	0.1617 ± 0.0042	0.816 ± 0.013	0.3739 ± 0.0089	0.3100 ± 0.0070
A0105-11(F)	**[0.0395 mg]**								
200 °C	5.78E-09			0.069 ± 0.010	0.995 ± 0.030	0.1531 ± 0.0059	0.798 ± 0.052	0.384 ± 0.017	0.328 ± 0.026
1800 °C	1.97E-08	0.0022 ± 0.0015	0.0041 ± 0.0024	0.0826 ± 0.0044	1.055 ± 0.023	0.1615 ± 0.0052	0.838 ± 0.024	0.374 ± 0.011	0.317 ± 0.011
Total	2.55E-08	0.0022 ± 0.0015	0.0041 ± 0.0024	0.0795 ± 0.0041	1.041 ± 0.019	0.1596 ± 0.0042	0.829 ± 0.022	0.3761 ± 0.0090	0.319 ± 0.010

(Table S2 continued)

Sample&Temp.	^{132}Xe	^{124}Xe/^{132}Xe	^{126}Xe/^{132}Xe	^{128}Xe/^{132}Xe	^{129}Xe/^{132}Xe	^{130}Xe/^{132}Xe	^{131}Xe/^{132}Xe	^{134}Xe/^{132}Xe	^{136}Xe/^{132}Xe
Kyushu Univ. data									
A0105-14(F)	**[0.0057 mg]**								
200 °C	5.74E-09	0.013 ± 0.011	0.0073 ± 0.0073	0.084 ± 0.018	1.06 ± 0.15	0.170 ± 0.040	0.84 ± 0.12	0.373 ± 0.033	0.299 ± 0.052
1800 °C	7.55E-09			0.076 ± 0.022	0.830 ± 0.075	0.158 ± 0.013	0.824 ± 0.063	0.372 ± 0.024	0.346 ± 0.030
Total	1.33E-08	0.013 ± 0.011	0.0073 ± 0.0073	0.079 ± 0.015	0.930 ± 0.077	0.164 ± 0.019	0.831 ± 0.065	0.372 ± 0.020	0.326 ± 0.028
A0105-15(P)	**[0.1487 mg]**								
100 °C	6.52E-09	0.00242 ± 0.00073	0.0042 ± 0.0016	0.0741 ± 0.0044	1.028 ± 0.021	0.1580 ± 0.0048	0.823 ± 0.016	0.374 ± 0.013	0.312 ± 0.011
200 °C	8.32E-10	0.0079 ± 0.0058	0.0035 ± 0.0027	0.088 ± 0.023	1.034 ± 0.084	0.164 ± 0.019	0.808 ± 0.066	0.387 ± 0.028	0.322 ± 0.021
900 °C	3.63E-09	0.0066 ± 0.0031	0.0068 ± 0.0039	0.1016 ± 0.0078	1.366 ± 0.036	0.1890 ± 0.0089	0.949 ± 0.030	0.372 ± 0.022	0.311 ± 0.029
1800 °C	1.89E-08	0.00185 ± 0.00054	0.00323 ± 0.00063	0.0801 ± 0.0030	1.098 ± 0.016	0.1645 ± 0.0036	0.827 ± 0.017	0.3689 ± 0.0057	0.295 ± 0.011
Total	2.99E-08	0.00273 ± 0.00056	0.00388 ± 0.00071	0.0816 ± 0.0024	1.114 ± 0.012	0.1660 ± 0.0028	0.840 ± 0.012	0.3709 ± 0.0054	0.3017 ± 0.0083
A0105-15(F)	**[0.0035 mg]**								
200 °C	6.26E-09			0.099 ± 0.026	0.88 ± 0.13	0.150 ± 0.008	0.783 ± 0.091	0.398 ± 0.033	0.357 ± 0.019
1800 °C	1.94E-08	0.0113 ± 0.0072	0.0029 ± 0.0033	0.094 ± 0.011	1.17 ± 0.11	0.168 ± 0.040	0.833 ± 0.090	0.391 ± 0.017	0.286 ± 0.033
Total	2.57E-08	0.0113 ± 0.0072	0.0029 ± 0.0033	0.095 ± 0.011	1.097 ± 0.087	0.164 ± 0.031	0.821 ± 0.072	0.393 ± 0.015	0.303 ± 0.025
A0105-15 weighted average	2.98E-08	0.00292 ± 0.00057	0.00386 ± 0.00070	0.0819 ± 0.0024	1.113 ± 0.012	0.1660 ± 0.0028	0.840 ± 0.012	0.3714 ± 0.0053	0.3017 ± 0.0082
C0106-03(F)	**[0.0032 mg]**								
200 °C	3.20E-09			0.083 ± 0.040	1.07 ± 0.18	0.165 ± 0.051	0.804 ± 0.176	0.394 ± 0.061	0.309 ± 0.099
1800 °C	1.96E-08	0.0100 ± 0.0085	0.0018 ± 0.0076	0.081 ± 0.023	1.108 ± 0.122	0.174 ± 0.027	0.831 ± 0.081	0.394 ± 0.059	0.315 ± 0.030
Total	2.28E-08	0.0100 ± 0.0085	0.0018 ± 0.0076	0.081 ± 0.020	1.10 ± 0.11	0.173 ± 0.024	0.827 ± 0.074	0.394 ± 0.051	0.314 ± 0.029
C0106-04(F)	**[0.0028 mg]**								
200 °C	4.49E-09	0.0133 ± 0.0173	0.026 ± 0.015	0.071 ± 0.041	0.88 ± 0.14	0.164 ± 0.027	0.835 ± 0.149	0.343 ± 0.021	0.303 ± 0.030
1800 °C	1.78E-08	0.0154 ± 0.0121	0.0050 ± 0.0057	0.100 ± 0.032	1.063 ± 0.089	0.180 ± 0.016	0.838 ± 0.107	0.377 ± 0.039	0.310 ± 0.034
Total	2.23E-08	0.015 ± 0.010	0.0093 ± 0.0054	0.094 ± 0.027	1.025 ± 0.076	0.177 ± 0.014	0.837 ± 0.091	0.370 ± 0.032	0.309 ± 0.027
C0106-8(P)	**[0.1020 mg]**								
200 °C	4.83E-09	0.00199 ± 0.00132	0.0044 ± 0.0019	0.0669 ± 0.0071	0.980 ± 0.042	0.1531 ± 0.0094	0.790 ± 0.028	0.3780 ± 0.0097	0.327 ± 0.016
1800 °C	2.04E-08	0.00156 ± 0.00062	0.00291 ± 0.00056	0.0761 ± 0.0040	1.320 ± 0.030	0.1602 ± 0.0035	0.817 ± 0.014	0.3831 ± 0.0071	0.3188 ± 0.0053
Total	2.52E-08	0.00165 ± 0.00056	0.00319 ± 0.00059	0.0743 ± 0.0035	1.255 ± 0.025	0.1588 ± 0.0034	0.812 ± 0.013	0.3821 ± 0.0061	0.3203 ± 0.0053

Sample	^{132}Xe	^{124}Xe/^{132}Xe	^{126}Xe/^{132}Xe	^{128}Xe/^{132}Xe	^{129}Xe/^{132}Xe	^{130}Xe/^{132}Xe	^{131}Xe/^{132}Xe	^{134}Xe/^{132}Xe	^{136}Xe/^{132}Xe
CRPG-Nancy data									
A0105-05	**[0.140 mg]**								
Total	1.70E-08	0.004558 ± 0.000090	0.004032 ± 0.000085	0.08344 ± 0.00083	1.0672 ± 0.0078	0.1614 ± 0.0014	0.8240 ± 0.0050	0.3863 ± 0.0031	0.3267 ± 0.0026

(Table S2 continued)

Sample & Temp.	^{132}Xe	^{124}Xe/^{132}Xe	^{126}Xe/^{132}Xe	^{128}Xe/^{132}Xe	^{129}Xe/^{132}Xe	^{130}Xe/^{132}Xe	^{131}Xe/^{132}Xe	^{134}Xe/^{132}Xe	^{136}Xe/^{132}Xe
ETH data									
A0105-02	**[0.1589 mg]**								
step-1	1.92E-08	0.00486 ± 0.00021	0.00405 ± 0.00027	0.0800 ± 0.0014	1.0457 ± 0.0056	0.1602 ± 0.0020	0.8080 ± 0.0044	0.3853 ± 0.0032	0.3279 ± 0.0025
step-2	5.62E-09	0.00548 ± 0.00054	0.00464 ± 0.00054	0.0830 ± 0.0021	1.062 ± 0.012	0.1681 ± 0.0031	0.8224 ± 0.0086	0.3798 ± 0.0047	0.3270 ± 0.0052
step-3	2.20E-10	0.0033 ± 0.0033		0.049 ± 0.017	0.86 ± 0.10	0.147 ± 0.034	0.674 ± 0.076	0.431 ± 0.060	0.265 ± 0.059
Total	2.50E-08	0.00499 ± 0.00021	0.00415 ± 0.00024	0.0804 ± 0.0012	1.0477 ± 0.0052	0.1618 ± 0.0017	0.8100 ± 0.0039	0.3845 ± 0.0027	0.3271 ± 0.0023
C0106-01	**[0.1 mg]**								
step-1	1.47E-08	0.00467 ± 0.00032	0.00392 ± 0.00033	0.0806 ± 0.0016	1.030 ± 0.012	0.1566 ± 0.0030	0.817 ± 0.010	0.3819 ± 0.0057	0.3289 ± 0.0049
step-2	1.60E-10				0.95 ± 0.37		0.78 ± 0.27	0.20 ± 0.13	0.25 ± 0.11
Total	1.48E-08	0.00467 ± 0.00032	0.00392 ± 0.00033	0.0806 ± 0.0016	1.030 ± 0.013	0.1566 ± 0.0030	0.817 ± 0.010	0.3800 ± 0.0059	0.3280 ± 0.0050
Murchison	**[0.0632 mg]**								
step-1	1.35E-08	0.00427 ± 0.00043	0.00434 ± 0.00055	0.0784 ± 0.0029	1.065 ± 0.019	0.1594 ± 0.0037	0.812 ± 0.013	0.3788 ± 0.0065	0.3282 ± 0.0066
step-2	4.70E-10			0.094 ± 0.024	1.13 ± 0.15	0.216 ± 0.045	0.91 ± 0.14	0.429 ± 0.070	0.386 ± 0.066
Total	1.40E-08	0.00427 ± 0.00043	0.00434 ± 0.00055	0.0789 ± 0.0029	1.067 ± 0.019	0.1613 ± 0.0038	0.815 ± 0.013	0.3804 ± 0.0067	0.3302 ± 0.0067

Sample	^{132}Xe	^{124}Xe/^{132}Xe	^{126}Xe/^{132}Xe	^{128}Xe/^{132}Xe	^{129}Xe/^{132}Xe	^{130}Xe/^{132}Xe	^{131}Xe/^{132}Xe	^{134}Xe/^{132}Xe	^{136}Xe/^{132}Xe
Washington U. data									
A0105-04	**[0.1729 mg]**								
Total	2.31E-08	0.00450 ± 0.00007	0.00399 ± 0.00007	0.0796 ± 0.0006	1.0620 ± 0.0019	0.1609 ± 0.0006	0.8126 ± 0.0019	0.3817 ± 0.0010	0.3212 ± 0.0010
C0106-05	**[0.0817 mg]**								
Total	3.15E-08	0.00444 ± 0.00009	0.00378 ± 0.00010	0.0797 ± 0.0005	1.0365 ± 0.0023	0.1586 ± 0.0007	0.8093 ± 0.0019	0.3809 ± 0.0018	0.3231 ± 0.0013

Sample	Weight (µg)	^{132}Xe	^{124}Xe/^{132}Xe	^{126}Xe/^{132}Xe	^{128}Xe/^{132}Xe	^{129}Xe/^{132}Xe	^{130}Xe/^{132}Xe	^{131}Xe/^{132}Xe	^{134}Xe/^{132}Xe	^{136}Xe/^{132}Xe
U. Manchester data										
A0105-03	0.6	3.7E-09	0.0005 ± 0.0075	0.00714 ± 0.00634	0.082 ± 0.012	1.104 ± 0.034	0.1834 ± 0.0131	0.830 ± 0.029	0.3873 ± 0.0183	0.3218 ± 0.0153
A0105-12	2.7	5.3E-09	0.0042 ± 0.0012	0.00437 ± 0.00098	0.0826 ± 0.0025	1.0853 ± 0.0093	0.1644 ± 0.0030	0.816 ± 0.008	0.3832 ± 0.0048	0.3245 ± 0.0042
C0106-02	11.5	1.2E-08	0.00433 ± 0.00030	0.00404 ± 0.00026	0.08327 ± 0.00077	1.0498 ± 0.0032	0.1639 ± 0.0010	0.825 ± 0.003	0.3879 ± 0.0016	0.3235 ± 0.0014

Concentrations are given in cm^3STP/g, and their uncertainties (1σ) are ~10%. Values in parentheses are not corrected for blank gas. The sample mass of C0106-01 is tentatively assumed to be 0.1 mg. Errors are 1σ.

Table S3. Bulk nitrogen compositions of the Ryugu pellet samples.

Sample	N (ppm)	δ^{15}N (‰)	Laboratory
A0105-07	700 ± 10	+ 1.7 ± 0.5	Ibaraki U.
C0106-07	840 ± 5	0.0 ± 0.4	Ibaraki U.
A0105-05	890 ± 20	+18.1 ± 0.9	CRPG-Nancy
C0106-06	860 ± 10	+19.5 ± 0.9	CRPG-Nancy

The presented errors are 1σ.

Table S4. Estimated concentrations of cosmogenic ^{21}Ne and trapped ^{20}Ne in the Ryugu samples.

Sample & Temp.	model 1					model 2				
A0105-01(P)	cosm-^{21}Ne	SW-^{20}Ne	P1-^{20}Ne	HL-^{20}Ne	G-^{20}Ne	cosm-^{21}Ne	SW-^{20}Ne	P1-^{20}Ne	HL-^{20}Ne	G-^{20}Ne
100 °C	3.2	135		45		3.3	87	93		
200 °C	0.4	47		17		0.4	29	36		
900 °C	0.5		151	63		0.5		151	63	
1800 °C	0.4		181		0.6	0.4		181		0.6
Total	4.5	182	332	125	0.6	4.6	115	461	63	0.6

Sample & Temp.	model 1					model 2				
A0105-10(P)	cosm-^{21}Ne	SW-^{20}Ne	P1-^{20}Ne	HL-^{20}Ne	G-^{20}Ne	cosm-^{21}Ne	SW-^{20}Ne	P1-^{20}Ne	HL-^{20}Ne	G-^{20}Ne
100 °C	3.8	298		63		3.8	230	131		
200 °C	0.51	73		14		0.52	58	29		
900 °C	0.49		206	136		0.49		206	136	
1800 °C	1.4		142	5		1.39		142	5	
Total	6.1	371	348	218		6.2	289	507	141	

Sample & Temp.	model 1					model 2				
A0105-15(P)	cosm-^{21}Ne	SW-^{20}Ne	P1-^{20}Ne	HL-^{20}Ne	G-^{20}Ne	cosm-^{21}Ne	SW-^{20}Ne	P1-^{20}Ne	HL-^{20}Ne	G-^{20}Ne
100 °C		42338	10572			1.2	52888			18
200 °C		28358	8048			1.17	36388			14
900 °C		49885	18566			6.57	68412			32
1800 °C	1.1	391	1561			1.6	1949			3
Total	1.1	120972	38748			10.5	159636			67

Sample & Temp.	model 1					model 2				
C0106-8(P)	cosm-^{21}Ne	SW-^{20}Ne	P1-^{20}Ne	HL-^{20}Ne	G-^{20}Ne	cosm-^{21}Ne	SW-^{20}Ne	P1-^{20}Ne	HL-^{20}Ne	G-^{20}Ne
200 °C	4.8	57	240			4.7	181		116	
1800 °C	1.6		80	315		1.6		80	315	
Total	6.4	57	319	315		6.3	181	80	430	

Sample & Temp.	model 1					model 2				
A0105-06(F)	cosm-^{21}Ne	SW-^{20}Ne	P1-^{20}Ne	HL-^{20}Ne	G-^{20}Ne	cosm-^{21}Ne	SW-^{20}Ne	P1-^{20}Ne	HL-^{20}Ne	G-^{20}Ne
200 °C	2.4	6476		655		3.1	5774	1357		
1800 °C	2.5	1857		681		3.3	1126	1411		
Total	5.0	8333		1336		6.4	6900	2767		

Sample & Temp.	model 1					model 2				
A0105-08(F)	cosm-^{21}Ne	SW-^{20}Ne	P1-^{20}Ne	HL-^{20}Ne	G-^{20}Ne	cosm-^{21}Ne	SW-^{20}Ne	P1-^{20}Ne	HL-^{20}Ne	G-^{20}Ne
200 °C	4.8	454				4.8	454			
1800 °C	2.9		290	130		2.8	150		270	
Total	7.7	454	290	130		7.6	604		270	

Sample & Temp.	model 1					model 2				
A0105-10(F)	cosm-^{21}Ne	SW-^{20}Ne	P1-^{20}Ne	HL-^{20}Ne	G-^{20}Ne	cosm-^{21}Ne	SW-^{20}Ne	P1-^{20}Ne	HL-^{20}Ne	G-^{20}Ne
200 °C	3.1	405		97		3.1	405		97	
600 °C										
1800 °C			404		0.35	0.1	403			1.0
Total	3.1	405	404	97	0.35	3.2	808		97	1.0

Sample & Temp.	model 1					model 2				
A0105-11(F)	cosm-^{21}Ne	SW-^{20}Ne	P1-^{20}Ne	HL-^{20}Ne	G-^{20}Ne	cosm-^{21}Ne	SW-^{20}Ne	P1-^{20}Ne	HL-^{20}Ne	G-^{20}Ne
200 °C	6.9	573		47		6.9	573		47	
1800 °C	1.5		203	261		1.4	105		359	
Total	8.4	573	203	308		8.3	678		406	

Sample & Temp.	model 1					model 2				
A0105-14(F)	cosm-^{21}Ne	SW-^{20}Ne	P1-^{20}Ne	HL-^{20}Ne	G-^{20}Ne	cosm-^{21}Ne	SW-^{20}Ne	P1-^{20}Ne	HL-^{20}Ne	G-^{20}Ne
200 °C	4.3	68		120		4.3	68		120	
1800 °C	1.4	24	264			1.2	161		128	
Total	5.7	92	264	120		5.5	229		248	

(Table S4 continued)

Sample & Temp.	model 1					model 2				
A0105-15(F)	cosm-^{21}Ne	SW-^{20}Ne	P1-^{20}Ne	HL-^{20}Ne	G-^{20}Ne	cosm-^{21}Ne	SW-^{20}Ne	P1-^{20}Ne	HL-^{20}Ne	G-^{20}Ne
200 °C		38559	19484			3.7	58001			34
1800 °C	0.8	42927	24475			9.7	67350			42
Total	0.8	81485	43959			13	125350			76

Sample & Temp.	model 1					model 2				
C0106-03(F)	cosm-^{21}Ne	SW-^{20}Ne	P1-^{20}Ne	HL-^{20}Ne	G-^{20}Ne	cosm-^{21}Ne	SW-^{20}Ne	P1-^{20}Ne	HL-^{20}Ne	G-^{20}Ne
200 °C	3.3	605	179			3.2	697		86	
1800 °C	1.8	722		386		1.8	722		386	
Total	5.1	1327	179	386		5.0	1419		472	

Sample & Temp.	model 1					model 2				
C0106-04(F)	cosm-^{21}Ne	SW-^{20}Ne	P1-^{20}Ne	HL-^{20}Ne	G-^{20}Ne	cosm-^{21}Ne	SW-^{20}Ne	P1-^{20}Ne	HL-^{20}Ne	G-^{20}Ne
200 °C	2.6	348	224			2.5	464		108	
1800 °C	1.9	221		108		1.9	221		108	
Total	4.5	569	224	108		4.4	685		216	

Sample & Temp.	model 1					model 2				
A0105-05	cosm-^{21}Ne	SW-^{20}Ne	P1-^{20}Ne	HL-^{20}Ne	G-^{20}Ne	cosm-^{21}Ne	SW-^{20}Ne	P1-^{20}Ne	HL-^{20}Ne	G-^{20}Ne
step-1	3.4	372		213		3.7	144	441		
step-2	0.3		166	159		0.3		166	159	
Total	3.7	372	166	372		3.9	144	607	159	

Sample & Temp.	model 1					model 2				
C0106-06	cosm-^{21}Ne	SW-^{20}Ne	P1-^{20}Ne	HL-^{20}Ne	G-^{20}Ne	cosm-^{21}Ne	SW-^{20}Ne	P1-^{20}Ne	HL-^{20}Ne	G-^{20}Ne
step-1	3.3	24	325			3.1	192		157	
step-2	0.0			53	0.2	0.0			53	0.2
step-3	0.1		44	3		0.1		44	3	
Total	3.4	24	369	56	0.2	3.3	192	44	213	0.2

Sample & Temp.	model 1					model 2				
A0105-02	cosm-^{21}Ne	SW-^{20}Ne	P1-^{20}Ne	HL-^{20}Ne	G-^{20}Ne	cosm-^{21}Ne	SW-^{20}Ne	P1-^{20}Ne	HL-^{20}Ne	G-^{20}Ne
step-1	4.2	148		381		4.4		285	243	
step-2	0.05	11		5		0.05	5	11		
step-3	0.1		14		0.03	0.1		15		0.03
Total	4.4	159	14	386	0.03	4.5	5	311	243	0.03

Sample & Temp.	model 1					model 2				
C0106-01	cosm-^{21}Ne	SW-^{20}Ne	P1-^{20}Ne	HL-^{20}Ne	G-^{20}Ne	cosm-^{21}Ne	SW-^{20}Ne	P1-^{20}Ne	HL-^{20}Ne	G-^{20}Ne
step-1	(1.6)	(65)		(169)		(1.7)		(126)	(108)	
step-2										
Total	(1.6)	(65)		(169)		(1.7)		(126)	(108)	

Sample & Temp.	model 1					model 2				
A0105-04	cosm-^{21}Ne	SW-^{20}Ne	P1-^{20}Ne	HL-^{20}Ne	G-^{20}Ne	cosm-^{21}Ne	SW-^{20}Ne	P1-^{20}Ne	HL-^{20}Ne	G-^{20}Ne
low temp.	3.9	335		135		4.0	190	280		
high temp.	0.7		22	197		1.0		218		0.4
Total	4.6	335	22	332		5.0	190	498		0.4

Sample & Temp.	model 1					model 2				
C0106-05	cosm-^{21}Ne	SW-^{20}Ne	P1-^{20}Ne	HL-^{20}Ne	G-^{20}Ne	cosm-^{21}Ne	SW-^{20}Ne	P1-^{20}Ne	HL-^{20}Ne	G-^{20}Ne
low temp.	2.7	405		304		3	78	631		
high temp.	0.8			440	0.2	1.5		439		1
Total	3.5	405		744	0.2	4.5	78	1070		1

Concentrations are given in 10^{-9} cm^{3}STP/g, and their uncertainties (1σ) are ~10% (uncertainties of end members' compositions are not considered). Abundances of each component were calculated by assuming a mixture of three components, one cosmogenic (cosm)-produced and two trapped Ne components for each extraction step. Two models are shown because it is difficult to determine the two trapped components appropriate. The concentrations of cosm-^{21}Ne

is less affected by the assumption of the trapped components. The values for C0106-01 in the parentheses are preliminary because its sample weight is not determined yet (*13*).